Human Molecular Genetics, 2015, Vol. 24, No. 18 5154–5173

doi: 10.1093/hmg/ddv238
Advance Access Publication Date: 30 June 2015
Original Article

ORIGINAL ARTICLE

PABPN1 suppresses TDP-43 toxicity in ALS disease models

Ching-Chieh Chou[1,2], Olga M. Alexeeva[1], Shizuka Yamada[3], Amy Pribadi[3], Yi Zhang[1,4], Bi Mo[1], Kathryn R. Williams[1], Daniela C. Zarnescu[3] and Wilfried Rossoll[1,2,*]

[1]Department of Cell Biology, [2]Center for Neurodegenerative Disease, Emory University School of Medicine, Atlanta, GA 30322, USA, [3]Department of Molecular and Cellular Biology, University of Arizona, Tucson, AZ 85721, USA and [4]Department of Neurology, Xiangya Hospital, Central South University, Changsha, Hunan, China

*To whom correspondence should be addressed. Email: wrossol@emory.edu

Abstract

TAR DNA-binding protein 43 (TDP-43) is a major disease protein in amyotrophic lateral sclerosis (ALS) and related neurodegenerative diseases. Both the cytoplasmic accumulation of toxic ubiquitinated and hyperphosphorylated TDP-43 fragments and the loss of normal TDP-43 from the nucleus may contribute to the disease progression by impairing normal RNA and protein homeostasis. Therefore, both the removal of pathological protein and the rescue of TDP-43 mislocalization may be critical for halting or reversing TDP-43 proteinopathies. Here, we report poly(A)-binding protein nuclear 1 (PABPN1) as a novel TDP-43 interaction partner that acts as a potent suppressor of TDP-43 toxicity. Overexpression of full-length PABPN1 but not a truncated version lacking the nuclear localization signal protects from pathogenic TDP-43-mediated toxicity, promotes the degradation of pathological TDP-43 and restores normal solubility and nuclear localization of endogenous TDP-43. Reduced levels of PABPN1 enhances the phenotypes in several cell culture and *Drosophila* models of ALS and results in the cytoplasmic mislocalization of TDP-43. Moreover, PABPN1 rescues the dysregulated stress granule (SG) dynamics and facilitates the removal of persistent SGs in TDP-43-mediated disease conditions. These findings demonstrate a role for PABPN1 in rescuing several cytopathological features of TDP-43 proteinopathy by increasing the turnover of pathologic proteins.

Introduction

TAR-DNA-binding protein 43 (TDP-43) has emerged as a key player in the pathogenesis of neurodegenerative diseases, based on genetic and pathological studies (1). TDP-43 has first been identified as a major component of abnormal cytoplasmic aggregates in amyotrophic lateral sclerosis (ALS) and frontotemporal lobar degeneration (FTLD) (2,3). The vast majority of both familial and sporadic ALS cases (ca. 97%) and the most common type of FTLD (ca. 45%), now classified as FTLD-TDP, are characterized by TDP-43 pathology and are now recognized as belonging to the same disease spectrum (4). A direct causal link was established by the discovery of >30 different missense mutations in exon 6 of the *TARDBP* gene encoding TDP-43, accounting for ca. 4% of inherited and 1.5% of sporadic ALS cases and rare patients with FTLD-TDP (5). Pathologic accumulation of TDP-43 in ubiquitin-positive aggregates was subsequently found in a variety of neurodegenerative diseases including Alzheimer's disease (AD), Parkinson's disease and Huntington's disease (6,7), indicating that TDP-43 proteinopathy may contribute broadly to neurodegeneration.

TDP-43 is an RNA-binding protein that shares a similar structure with heterogeneous nuclear ribonucleoproteins (8). TDP-43 contains two RNA-recognition motifs and a Q/N-rich prion-like C-terminal region, which makes it intrinsically aggregation-prone

Received: February 23, 2015. **Revised:** May 24, 2015. **Accepted:** June 22, 2015

and plays a key role in pathogenesis (9). TDP-43 is predominantly expressed in the nucleus but can shuttle between nuclear and cytoplasmic compartments and plays multiple roles in RNA processing in both compartments (10). The disease-associated changes found in ALS and FTLD-TDP cases include aberrant aggregation of ubiquitinated and hyperphosphorylated TDP-43, the accumulation of truncated 20–25 kDa TDP43 C-terminal fragments (TDP-CTFs), cytoplasmic mislocalization and loss of TDP-43 from the nucleus. Various cellular stress factors cause TDP-43 to localize in cytoplasmic stress granules (SGs) as a normal physiological response (11–13). It has been speculated that chronic and prolonged SG formation may be an initiating event triggering irreversible TDP-43 inclusion pathology (14–16). TDP-43 inclusion pathology may reflect an exaggeration of normal accumulation of TDP-43 into cytoplasmic RNA granules under disease-associated mutations (17,18) or stressful conditions (15). While the effect of hyperphosphorylation on the properties of TDP-43 is still controversial, it may modulate the oligomerization (19,20) and increase protease resistance (21). Not only are proteins that target proteins for degradation present in TDP-43 aggregates but mutations in several genes affecting protein degradation cause ALS/FTLD-TDP characterized by TDP-43 aggregation. Taken together, these studies implicate a failure of TDP-43 clearance via autophagy and/or the ubiquitin-proteasome system (UPS) in human ALS/FTLD-TDP (22). The biological role of TDP-43 in RNA processing and the fact that TDP-43 accumulation can be triggered by a dysfunction of protein degradation pathways support the hypothesis that disruption of both RNA and protein homeostasis are central to ALS pathogenesis (23).

ALS and other TDP-43 proteinopathies are characterized by both the formation of TDP-43 containing aggregates in the cytoplasm and the loss of normal TDP-43 from the nucleus (2). Numerous studies have provided evidence for a toxic gain-of-function of pathologic TDP-43 that accumulates in the cytoplasm (24). Overexpression of wild-type or mutant TDP-43 in neurons has been shown to mimic key features of TDP-43 proteinopathy *in vitro*, including the sequestration of RNA-binding proteins into detergent-insoluble aggregates (25,26). Especially expression of TDP-CTF, a C-terminal fragment of TDP-43 from aa 208–414 found in ALS/FTLD-TDP patients, recapitulates key features of TDP-43 proteinopathy in transfected neurons (27,28). Other studies show that similarly, partial loss of TDP-43 can cause progressive neurodegeneration phenotypes similar to ALS (29,30). Taken together, this suggests that the toxic gain-of-function and the loss-of-function hypotheses are not mutually exclusive and could both contribute to neurodegeneration (31–34). This also suggests that targeting the deleterious effects of TDP-43 proteinopathy requires both the removal of pathological cytoplasmic TDP-43 and the restoration of nuclear TDP-43 levels.

Here, we report poly(A)-binding protein nuclear 1 (PABPN1, also known as PABP2) as a novel modifier of TDP-43 proteinopathy in several *in vitro* and *in vivo* models of ALS and FTLD-TDP. PABPN1 is thought to function during post-transcriptional processing of RNA in the nucleus, regulating polyadenylation and nuclear export of mRNAs, and the turnover of lncRNA (35). Expansion of an N-terminal polyalanine repeat region causes the muscle disease oculopharyngeal muscular dystrophy (OPMD), which is also characterized by the presence of TDP-43-positive aggregates (36), suggesting a potential functional link between TDP-43 and PABPN1. In this study, we identified PABPN1 as a novel direct interaction partner of TDP-43 that also acts as a potent suppressor for TDP-43-induced toxicity, whereas the loss of PABPN1 conversely enhances the phenotype in various models of TDP-43 proteinopathy ranging from yeast to *Drosophila* and mammalian primary neurons. PABPN1 overexpression strongly reduces protein levels of exogenously expressed ALS patient-specific mutant and truncated TDP-43 but only weakly affects wild-type TDP-43. PABPN1 does not change levels of endogenous full-length TDP-43, and restores its solubility and proper nuclear localization under disease conditions. Our data show that increased protein turnover of pathological TDP-43 by PABPN1 is mainly mediated via the UPS. In addition, PABPN1 rescues the dysregulation of SG dynamics in TDP-43-mediated disease conditions. In summary, PABPN1 acts as a protective modifier across various cell culture and animal models of TDP-43 proteinopathy by rescuing important disease phenotypes.

Results

TDP-43 is a novel interaction partner of PABPN1

In a yeast two-hybrid screen for proteins that directly interact with human TDP-43 (hTDP-43), in addition to known TDP-43-associated proteins such as hnRNPA3, we also identified PABPN1 as a putative novel interaction partner. PABPN1 is a ubiquitously expressed protein that is involved in processive polyadenylation of pre-mRNA transcripts (35). PABPN1 shares similarity with RNA regulatory proteins and interacts with hnRNP-A1 and A2/B1 (37), as well as its nuclear import receptor transportin (38) and poly(A) polymerase (39). To verify the yeast two-hybrid interaction, we cloned full-length hTDP-43 and PABPN1 into bait and prey vectors. Both proteins were able to homodimerize as reported previously (40,41), but also showed specific interactions with each other (Table 1).

To confirm the protein–protein interaction in mammalian cells, we co-transfected Neuro-2a (N2a) neuroblastoma cells with expression constructs for FLAG-tagged TDP-43, and GFP-tagged full-length or truncated PABPN1 (full length: FL; deletion of C-terminal nuclear localization signal (NLS) 18aa: ΔNLS18; deletion of C-terminal 50aa: ΔNLS50) (Fig. 1A). The C-terminus of PABPN1 is highly enriched in methylated arginine residues and contains an NLS (42). Deletion of the last 18aa partially inactivated the NLS function and caused uniform nucleocytoplasmic distribution, whereas deletion of the last 50aa led to cytoplasmic localization (Fig. 1B). FLAG-tagged TDP-43 associates with full-length PABPN1 and to a lesser degree with PABPN1$^{\Delta NLS50}$ and PABPN1$^{\Delta NLS18}$, demonstrating that the C-terminal region of PABPN1 is not essential for their interaction (Fig. 1C). Treatment with RNaseA did not abolish the association between TDP-43 and PABPN1, showing that this interaction is not mediated via RNA.

Table 1. TDP-43 and PABPN1 interact in yeast two-hybrid assays

	Activation domain pGADT7 *vector*	hPABPN1	hTDP-43
Binding domain			
pGBKT7 *vector*	—	—	—
hPABPN1	—	++	+
hTDP-43	—	+	+++

Full-length hTDP-43 and PABPN1 (hPABPN1) were cloned into yeast two-hybrid vectors and co-transformed into a reporter strain. Columns represent empty pGADT7 prey vector and hPABPN1 and hTDP-43 cloned into pGADT7, respectively; rows represent empty pGBKT7 bait vector and hPABPN1 and hTDP-43 cloned into pGBKT7, respectively. Strength of interaction was measured by scoring growth on selective media (SD/–Ade/–His/–Leu/–Trp) from weak (+) to strong (+++). Both TDP-43 and PABPN1 interact with themselves (indicating dimerization) but also with each other.

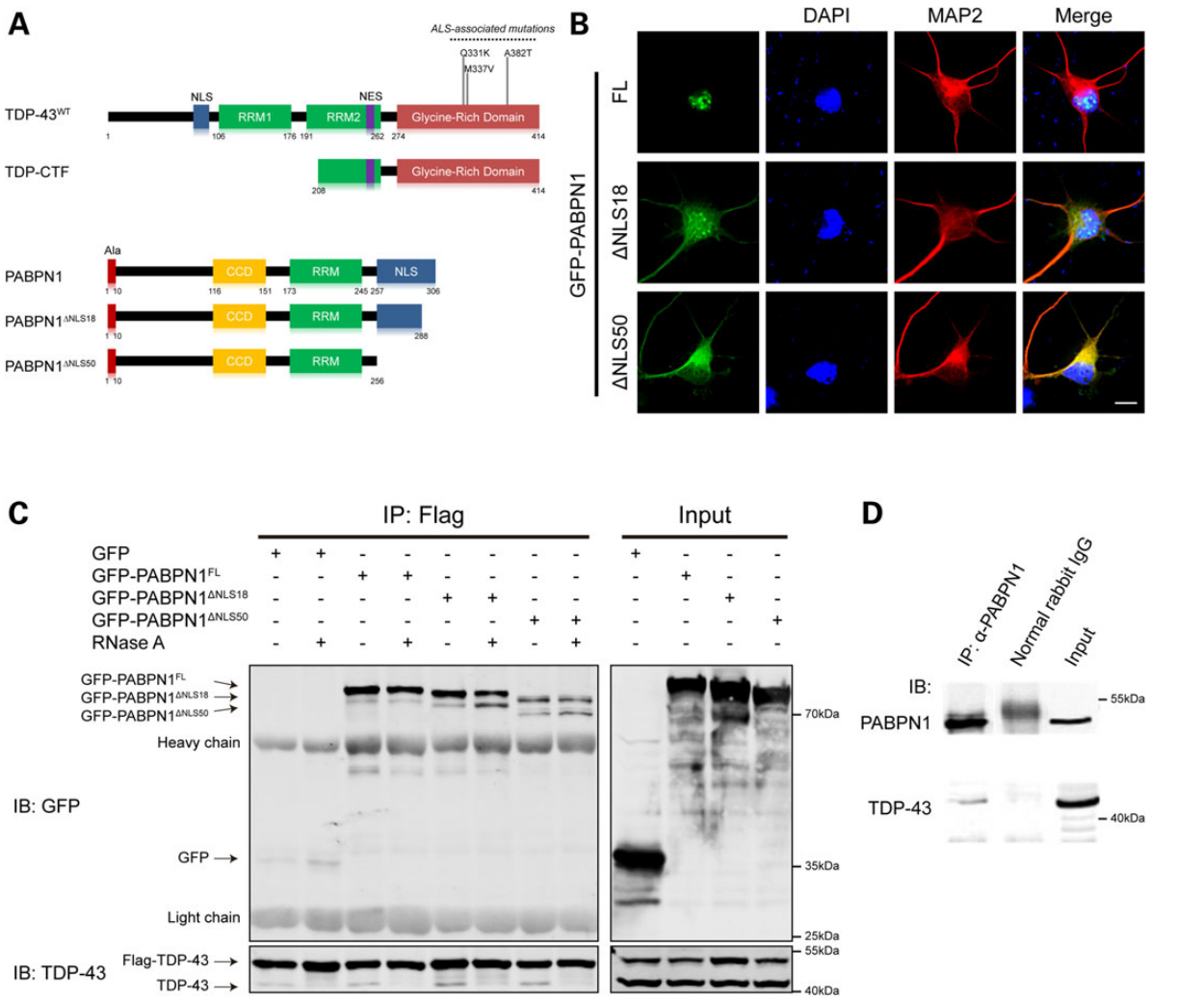

Figure 1. TDP-43 and PABPN1 associate by protein–protein interaction in mammalian cells and tissue. (**A**) Schematic domain structures of hTDP-43 and PABPN1 constructs used in this study. (Top) Human TDP-43 protein contains an NLS, two RNA-recognition motifs, a nuclear export sequence and a glycine-rich C-terminal domain where the majority of ALS-associated mutations are located. We cloned fusion constructs of wild-type TDP-43, the ALS-specific missense mutations Q331K, M337V and A382T, and a C-terminal fragment from aa 208–414 (TDP-CTF) that accumulates as a cleavage product in ALS and FTLD-TDP patient tissue. (Bottom) Human PABPN1 contains an N-terminal stretch of 10 alanines (Ala), a coiled-coil domain, one RRM domain and an NLS in the arginine-rich C-terminus. We use two C-terminal truncation mutations of PABPN1 with a partial (aa 289–306, PABPN1$^{\Delta NLS18}$) or full deletion of the NLS region (aa 257–306, PABPN1$^{\Delta NLS50}$). (**B**) Localization of PABPN1 constructs in primary motor neurons. Fluorescence microscopy images show that GFP-PABPN1 is predominantly localized in the nucleus. GFP-PABPN1$^{\Delta NLS18}$ shows nucleocytoplasmic localization, whereas GFP-PABPN1$^{\Delta NLS50}$ is confined to the cytoplasm. Scale bar: 10 µm. (**C**) Association of PABPN1 with TDP-43 in transfected N2a cells. (Left panel) Western blot analysis of anti-FLAG immunoprecipitates from N2a cells co-expressing FLAG-tagged TDP-43 and GFP or GFP-tagged PABPN1 shows association of TDP-43 with PABPN1 that is independent of RNA-binding or the presence of the PABPN1 C-terminal region (full length: FL; ΔNLS18 and ΔNLS50). RNase A treatment is indicated. Right panel: western blot analysis of cell lysates (input). (**D**) Association of TDP-43 with PABPN1 in mouse brain tissue. Western blot analysis of anti-PABPN1 immunoprecipitates from mouse brain lysates with anti-TDP-43 confirms the specific association of both proteins.

The C-terminal fragment TDP-CTF was also found to specifically associate with full-length PABPN1 in pulldown assays (Supplementary Material, Fig. S1). To verify association of the endogenous proteins, we used anti-PABPN1 antibodies to co-immunoprecipitate endogenous TDP-43 from embryonic mouse brain lysates (Fig. 1D). Taken together, our results identify PABPN1 as a novel direct interaction partner of TDP-43.

PABPN1 modulates TDP-43 toxicity in yeast and primary neuron models of TDP-43 proteinopathy

The budding yeast *Saccharomyces cerevisiae* has emerged as an important tool for investigating protein misfolding as a cause of several human neurodegenerative disorders, including a yeast model for TDP-43 proteinopathy (43–45). Remarkably, overexpression of hTDP-43 in yeast triggers spontaneous formation of aggregates similar to those observed in degenerating neurons of ALS patients (43). To determine whether PABPN1 can modulate TDP-43 toxicity in the yeast model, we performed spotting assays with a yeast strain transformed with expression plasmids for yellow and cyan fluorescent protein-tagged hTDP-43 and PABPN1 (hPABPN1) under control of the galactose-inducible GAL1 promoter. Inducing strong overexpression of hTDP-43-YFP from a multicopy plasmid resulted in dramatic inhibition of yeast growth as compared with a control plasmid expressing YFP alone (43). Importantly, we found that whereas mCerulean-hPABPN1 alone only weakly inhibited proliferation, it strongly mitigated the toxic effect of hTDP-43 on cell growth (Fig. 2A).

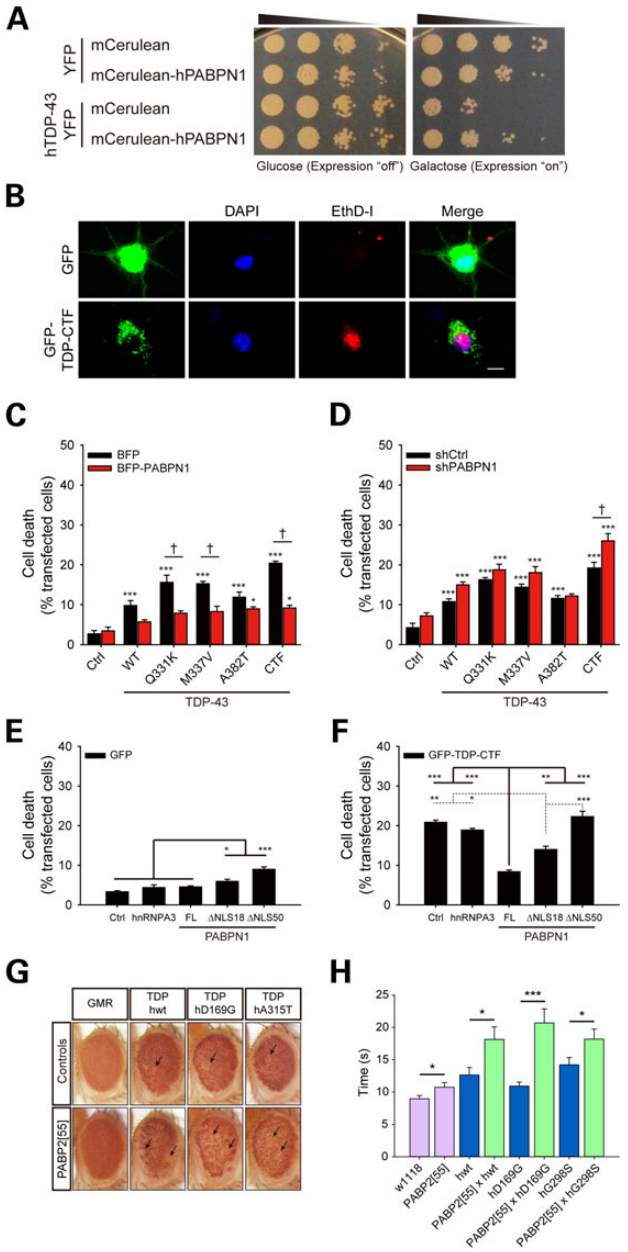

Figure 2. PABPN1 modulates TDP-43 toxicity in several *in vitro* and *in vivo* models of TDP-43 proteinopathy. (**A**) TDP-43 and PABPN1 toxicity in yeast. Spotting assays were used to measure cellular growth in yeast co-expressing hTDP-43 fused with yellow fluorescent protein (YFP) or the YFP control, together with monomeric Cerulean fluorescent protein-tagged human PABPN1 (mCerulean-hPABPN1) or the mCerulean control. Co-expression of PABPN1 strongly suppressed TDP-43 toxicity. (**B**) Cell death assay with the membrane-impermeable DNA-binding fluorescent EthD-I. Fluorescence microscopy of primary cortical neurons shows red fluorescent staining of nuclei in dead or dying cells when membranes are compromised. Cells were transfected with expression plasmids for GFP (top) or GFP-TDP-CTF (bottom). Scale bar: 10 µm. (**C**) Quantification of TDP-43-mediated cell death upon overexpression of PABPN1. Neurons were transfected with GFP control (Ctrl), and GFP-tagged hwt TDP-43 (TDP-43^{WT}), ALS-specific mutant TDP-43 (TDP-43^{Q331K}, TDP-43^{M337V} and TDP-43^{A382T}) or TDP-CTF expression plasmids. Co-expression of blue fluorescent protein-tagged PABPN1 (BFP-PABPN1) but not the BFP control reduced TDP-43 toxicity. Statistical analysis was performed with two-way ANOVA and Bonferroni's *post hoc* test (five independent experiments, $^{*}P < 0.05$, $^{***}P < 0.001$, TDP-43 constructs versus Ctrl; $^{\dagger}P < 0.05$, BFP-PABPN1 versus BFP. BFP: Ctrl ($n = 564$), WT ($n = 517$), Q331K ($n = 341$), M337V ($n = 393$), A382T ($n = 350$), CTF ($n = 333$); BFP-PABPN1: Ctrl ($n = 509$), WT ($n = 529$), Q331K ($n = 378$), M337V ($n = 335$), A382T ($n = 352$), CTF ($n = 317$). (**D**) Quantification of TDP-43-mediated cell death upon knockdown of PABPN1. Neurons were transfected with BFP control (Ctrl) and BFP-tagged TDP-43 expression constructs. Co-expression of the PABPN1-specific shRNA construct (shPABPN1) but not the nonsilencing control (shCtrl) exacerbated TDP-43 toxicity. Statistical analysis was performed with two-way ANOVA and Bonferroni's *post hoc* test (five independent experiments, $^{*}P < 0.05$, $^{***}P < 0.001$, TDP-43 constructs versus Ctrl; $^{\dagger}P < 0.05$, shPABPN1 versus shCtrl. BFP: Ctrl ($n = 447$), WT ($n = 370$), Q331K ($n = 253$), M337V ($n = 265$), A382T ($n = 256$), CTF ($n = 379$); BFP-PABPN1: Ctrl ($n = 507$), WT ($n = 412$), Q331K ($n = 286$), M337V ($n = 288$), A382T ($n = 273$) and CTF ($n = 446$). (**E**) Quantification of cell death in neurons expressing hnRNPA3 or PABPN1 variants (full length: FL; lacking 18aa of NLS: ΔNLS18; lacking 50aa of NLS: ΔNLS50). Only expression of PABPN1$^{\Delta NLS50}$ led to increased cell death. Statistical analysis was performed with one-way ANOVA and Bonferroni's *post hoc* test (three independent experiments, $^{*}P < 0.05$, $^{**}P < 0.01$, $^{***}P < 0.001$. Ctrl ($n = 302$), hnRNPA3 ($n = 300$), FL ($n = 309$), ΔNLS18 ($n = 304$), ΔNLS50 ($n = 301$). (**F**) Quantification of cell death in neurons co-expressing TDP-CTF and hnRNPA3 or PABPN1 variants. PABPN1$^{\Delta NLS18}$ suppressed TDP-43 toxicity only weakly, whereas PABPN1$^{\Delta NLS50}$ and hnRNPA3 had no obvious effect. Statistical analysis was performed with one-way ANOVA and Bonferroni's *post hoc* test (three independent experiments, $^{*}P < 0.05$, $^{**}P < 0.01$ and $^{***}P < 0.001$. Ctrl ($n = 275$), hnRNPA3 ($n = 302$), FL ($n = 233$), ΔNLS18 ($n = 295$) and ΔNLS50 ($n = 280$)). (**G**) Neurodegeneration phenotype in the adult *Drosophila* retina. Overexpression of hwt or mutant TDP-43 (hwt, hD169G and hA315T) in photoreceptor neurons using the GMR Gal4 driver causes a depigmentation (arrows) phenotype in the retina ($n = 10$). The loss-of-function mutant of the *Drosophila* PABPN1 ortholog PABP2[55] enhanced TDP-43-dependent depigmentation phenotype (arrows). (**H**) Locomotor phenotype in *Drosophila* larvae. Overexpression of human transgene variants (hwt, hD169G and hG298S) in motor neurons driven by the D42 Gal4 driver causes a significant time delay to turn over following a ventral-up inversion in larval turning assays. The PABP2[55] mutation enhanced TDP-43-dependent locomotor defects ($n = 30$–47). $^{*}P < 0.05$, $^{***}P < 0.001$. Graphs represent mean and SEM.

The result demonstrates that PABPN1 acts as a potent suppressor of TDP-43 toxicity in a yeast model of TDP-43 proteinopathy.

Previously, we have shown that expression of GFP-TDP-CTF in primary motor neurons leads to the formation of cytoplasmic inclusions with the hallmarks of TDP-43 pathology (46). These aggregates stain positive for ubiquitin, hyperphosphorylated TDP-43 (Ser409/410), and the autophagy adapter SQSTM1/p62 (Supplementary Material, Fig. S2). To test further how PABPN1 expression affects neuronal TDP-43 proteinopathy models, primary cortical neurons were transfected with GFP-fusion constructs for wild-type TDP-43 (TDP-43^{WT}), disease-associated mutants (TDP-43^{Q331K}, TDP-43^{M337V} and TDP-43^{A382T}) or TDP-CTF and measured how rates of cell death were altered by co-overexpression of BFP-PABPN1. Cell death among the transfected neurons was determined by scoring the nuclear uptake of the fluorescent dye ethidium homodimer I (EthD-I) (Fig. 2B). Consistent with previous reports that mutant or truncated TDP-43-enhanced cellular toxicity in cultured cell lines (13,47), primary neurons (26,46,48) and animal models (34), expression of ALS-specific mutant TDP-43 and TDP-CTF was more toxic than TDP-43^{WT} and increased the percentage of cell death in transfected neurons (Control: 2.7 ± 0.8%; TDP-43^{WT}: 9.8 ± 1.2%; TDP-43^{Q331K}: 15.6 ± 1.8%; TDP-43^{M337V}: 15.3 ± 0.6%; TDP-43^{A382T}: 11.9 ± 1.3%; TDP-CTF: 20.4 ± 0.5%) (Fig. 2C). The co-overexpression of PABPN1 greatly reduced cell death induced by TDP-CTF and mutant TDP-43 by 55% (9.2 ± 0.7%) and ca. 45–49% (TDP-43^{Q331K}: 7.9 ± 0.6; TDP-43^{M337V}: 8.3 ± 1.3). The overexpression of PABPN1 itself was not toxic (3.4 ± 1.0) (Fig. 2C).

Based on this finding, we tested whether reducing PABPN1 level had an impact on TDP-43 toxicity. We employed two different PABPN1-specific shRNA constructs (shPABPN1), which efficiently decreased endogenous PABPN1 protein levels in western-blot analysis (Fig. 3C). Reduction of PABPN1 alone did not significantly

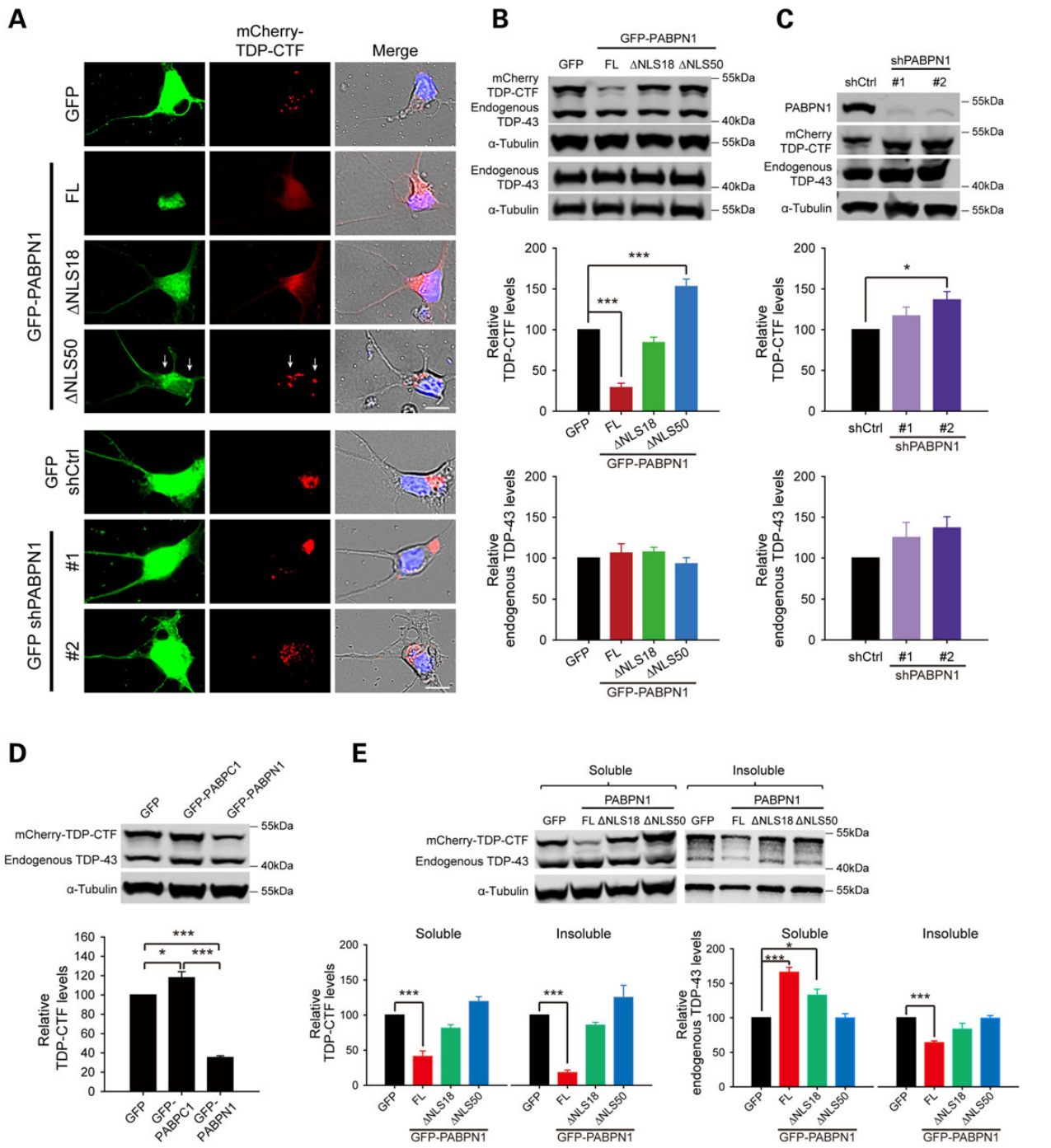

Figure 3. PABPN1 overexpression reduces pathological TDP-43 protein levels. (**A**) Fluorescence microscopy analysis of TDP-CTF aggregation. Top: Representative images of primary motor neurons expressing mCherry-TDP-CTF (red), and GFP-PABPN1 (FL, ΔNLS18 and ΔNLS50) (green). White arrows indicate co-aggregation of PABPN1$^{\Delta NLS50}$ with TDP-CTF in the cytoplasm. Bottom: Co-expression of mCherry-TDP-CTF with shRNA constructs encoding GFP. One control shRNA (shCtrl) and two shRNAs specific for PABPN1 knockdown (shPABPN1#1, shPABPN1#2) were used (green). Merged images show mCherry-TDP-CTF (red), nuclei (blue) and differential interference contrast. Scale bar: 10 µm. (**B** and **C**) Western blot analyses and quantification of TDP-CTF and endogenous TDP-43 protein levels in N2a cells after PABPN1 overexpression ($n = 7,7$) (B) or PABPN1 knockdown ($n = 7,6$) (C). Full-length PABPN1 and PABPN1$^{\Delta NLS50}$ expression had opposite effects on TDP-CTF levels. Statistical analysis was performed with one-way ANOVA and Bonferroni's *post hoc* test (*$P < 0.05$, ***$P < 0.001$). (**D**) Quantification of TDP-CTF protein levels upon overexpression of PABPC1 and PABPN1. Co-expression of mCherry-TDP-CTF with GFP, GFP-PABPC1 or GFP-PABPN1 in N2a cells showed opposite effects on TDP-CTF levels. Statistical analysis was performed with one-way ANOVA and Bonferroni's *post hoc* test (*$P < 0.05$, ***$P < 0.001$, $n = 5$). (**E**) Western blot analyses of detergent-soluble and insoluble protein fractions from N2a cells expressing TDP-CTF. PABPN1 overexpression reduced both soluble and insoluble TDP-CTF, statistical analysis with one-way ANOVA and Bonferroni's *post hoc* test (***$P < 0.001$, $n = 7$), and causes a shift of endogenous TDP-43 from insoluble to soluble form, statistical analysis with one-way ANOVA and Bonferroni's *post hoc* test (*$P < 0.05$, ***$P < 0.001$, $n = 7$).

affect rates of cell death (shCtrl: 4.2 ± 1.1; shPABPN1: 7.2 ± 0.8, $P > 0.99$), but enhanced TDP-CTF-induced cell death by 35% (shCtrl: 19.2 ± 1.6; shPABPN1: 26.0 ± 1.8, $P = 0.004$) (Fig. 2D).

To rule out an unspecific effect caused by overexpressing mRNA-binding proteins, we used as a control hnRNP-A3, a known TDP-43 associated protein that we have also identified

as a direct interaction partner of TDP-43 in our yeast two-hybrid screen. Co-overexpression of hnRNP-A3 was neither toxic, nor did it reduce TDP-CTF-induced cell death (Fig. 2E and F), suggesting a specific effect of PABPN1 overexpression on TDP-43 toxicity.

To find out whether nuclear localization of PABPN1 was required for suppression of TDP-43 toxicity, we co-expressed PABPN1 NLS mutants with TDP-CTF in primary neurons. Whereas nucleocytoplasmic PABPN1$^{\Delta NLS18}$ itself slightly increased cell death but acted as a weak suppressor of TDP-CTF-induced cell death, cytoplasmic PABPN1$^{\Delta NLS50}$ strongly enhanced cell death and had no positive effect on survival of TDP-CTF expressing cells (Fig. 2E and F). Our data suggest that ameliorating TDP-43 toxicity by PABPN1 requires its normal nuclear localization.

PABPN1 loss of function enhances TDP-43 toxicity in Drosophila models of ALS *in vivo*

Several groups have developed *Drosophila* models of ALS based on overexpression of hTDP-43 that recapitulate several aspects of pathology, including neurotoxicity, loss of motor neurons, locomotor dysfunction and reduced survival (49–54). To test the effect of PABPN1 in an *in vivo* model of TDP-43 proteinopathy, we employed several transgenic fly lines expressing human wild-type (hwt) or ALS-specific mutant TDP-43 (hA315T, hD169G) in the developing retina using the Gal4-UAS system (55). Overexpression of hwt and hA315T using the GMR Gal4 driver induced neurodegeneration in the adult retina that is visible as loss of pigmentation in the eye (54). When combined with a loss-of-function mutant of PABPN1 (PABP2[55]) (56), we observed that the loss of PABPN1 itself was not toxic, whereas it enhanced the TDP-43-induced neurodegeneration (Fig. 2G). As an additional assay, we used the motor neuron-specific D42 Gal4 driver to investigate locomotor dysfunction in larvae. Expression of the hwt and mutant alleles significantly increased the time the larva needed to turn back from the dorsal side and resume crawling on the ventral side (54,57). The PABPN1 loss-of-function genetic background exacerbated TDP-43-dependent locomotor defects (Fig. 2H). In summary, our results show that PABPN1 modulates TDP-43-mediated toxicity across several *in vitro* and *in vivo* genetic models of TDP-43 proteinopathy, acting as a protective modifier when overexpressed and enhancing TDP-43 toxicity when reduced.

PABPN1 specifically reduces protein levels of pathological TDP-43 in neuronal cell lines and primary neurons

The accumulation of pathological cytoplasmic inclusions containing TDP-43 is a key feature of ALS and FTLD-TDP (2,3). Normally, TDP-43 protein levels appear tightly regulated and even modest levels of overexpression can trigger neurodegeneration (23). Cytoplasmic mislocalization in combination with posttranslational modification, and the intrinsic aggregation propensity of TDP-43 may promote its accumulation in disease (31).

To investigate whether PABPN1 overexpression can reduce pathological TDP-43, N2a cells and primary motor neurons were transfected with TDP-CTF to induce formation of ubiquitinated and hyperphosphorylated aggregates (Supplementary Material, Fig. S2). Co-overexpression of PABPN1^{FL} significantly promoted the clearance of TDP-CTF by ~70%, whereas the truncated nucleocytoplasmic PABPN1$^{\Delta NLS18}$ lost the ability to reduce the pathological protein (Fig. 3A and B). PABPN1$^{\Delta NLS50}$ co-localized with TDP-CTF in the cytoplasm and enhanced the accumulation of TDP-CTF by 1.5-fold. Importantly, endogenous TDP-43 protein levels were not changed by PABPN1 (Fig. 3B). Furthermore, we assessed the effect of shRNA-mediated knockdown of PABPN1 on the protein level of TDP-CTF. Reducing PABPN1 levels exacerbated the accumulation of TDP-CTF but had no significant effect on endogenous TDP-43 (Fig. 3C).

To examine the specificity of PABPN1 for TDP-CTF, we co-overexpressed the TDP-43 associated mRNA-binding protein hnRNP-A3 as a negative control. HnRNP-A3 expression had no significant effect on TDP-CTF levels (Supplementary Material, Fig. S3A). Since a recent study has shown that the upregulation of the *Drosophila* poly(A)-binding protein cytoplasmic 1 (PABPC1) ortholog (dPABP) enhanced TDP-43 toxicity in a fly model of ALS and dPABP downregulation led to a slight reduction of cytoplasmic TDP-43 protein levels (58), we compared the effect of co-overexpressing either PABPN1 or PABPC1 on TDP-CTF protein accumulation in N2a cells. Indeed, PABPC1 exhibited an opposite role to PABPN1 by increasing TDP-CTF levels (PABPC1: 117.9 ± 6.1%; PABPN1: 35.1 ± 1.8%, $P < 0.001$) (Fig. 3D). Our results demonstrate an opposite role of nuclear and cytoplasmic poly(A)-binding proteins in modulating TDP-43 toxicity and protein accumulation.

To investigate whether PABPN1 may exhibit a general effect on pathologic protein inclusions, we used a model for pathogenic huntingtin (Htt) protein containing an expansion of poly-glutamine that causes Huntington's disease (59). To induce Htt aggregate formation, we co-transfected expression constructs for an N-terminal mutant Htt construct harboring 150 CAG repeats (mHtt) and PABPN1 into primary cortical neurons. PABPN1 did not alter the levels of aggregated mHtt suggesting a specific effect of PABPN1 on the removal of pathological TDP-43 instead of a more general effect on other pathological proteins (Supplementary Material, Fig. S3B).

To find out whether PABPN1 overexpression specifically targets both diffusely distributed TDP-CTF monomers and oligomers, as well as the larger insoluble aggregates, we partitioned TDP-CTF into detergent-soluble and -insoluble fractions. PABPN1^{FL} overexpression significantly reduced TDP-CTF protein levels in both fractions, whereas the cytoplasmic PABPN1$^{\Delta NLS50}$ truncation mutant did not show significant changes but a trend towards increasing levels of both soluble and insoluble TDP-CTF (Fig. 3E). Importantly, in cells expressing TDP-CTF, PABPN1 co-expression caused a shift of endogenous full-length TDP-43 from the insoluble to the soluble fraction, demonstrating that the clearance of pathologic TDP-CTF protein by PABPN1 restores the solubility of endogenous TDP-43 (Fig. 3E).

PABPN1 facilitates the clearance of pre-formed pathological TDP-43 aggregates

To find out whether PABPN1 overexpression acts by preventing the accumulation of pathologic TDP-CTF or whether it can also target existing aggregates in the cytoplasm, we performed time-lapse live-cell imaging experiments. Primary cortical neurons were co-transfected with constructs for expression of fluorescent protein-tagged TDP-CTF from the constitutive CMV promoter and PABPN1 from the doxycycline (Dox)-inducible Tet-ON promoter. Twenty-four hours after transfection, mCherry-TDP-CTF was strongly expressed in the cytoplasm and formed bright fluorescent foci indicating cytoplasmic aggregates. Then expression of GFP-PABPN1 was induced and the changes of mCherry-TDP-CTF levels were dynamically monitored by quantification of fluorescence intensity in time-lapse live-cell imaging (Fig. 4A and B). Whereas mCherry-TDP-CTF levels slightly increased over time in the vehicle group (120.2 ± 4.1%, $n = 20$) or GFP control groups (vehicle: 111.5 ± 5.2%; Dox: 120.6 ± 4.2%, $n = 20$), we observed a gradual reduction of mCherry-TDP-CTF levels (including the distinct

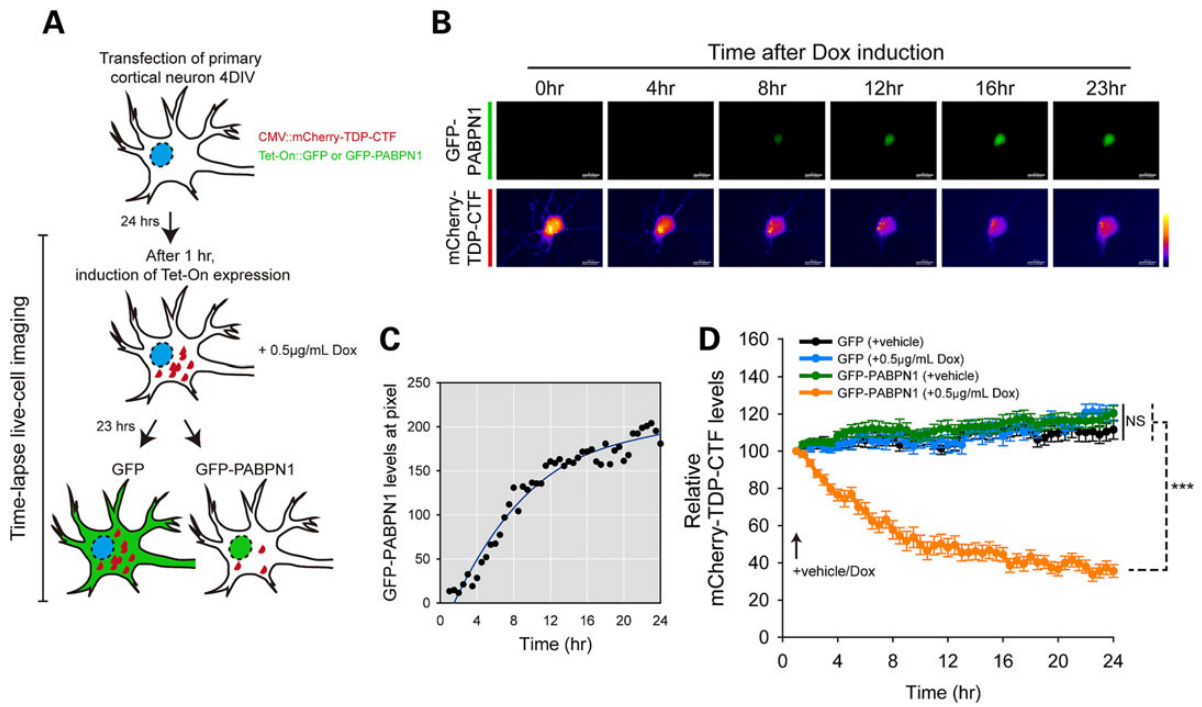

Figure 4. Induction of PABPN1 expression promotes the clearance of pre-formed pathological TDP-43 aggregates. (**A**) Schematic of time-lapse live-cell imaging to monitor TDP-CTF protein levels over time in the doxycycline (Dox)-inducible system. Primary cortical neurons were co-transfected with plasmids for constitutive CMV promoter-driven mCherry-TDP-CTF expression and inducible Tet-On promoter-driven GFP or GFP-PABPN1 expression. After 24 h, cells were imaged for 1 h to establish basal cellular TDP-CTF levels, and then GFP or GFP-PABPN1 expression were induced by adding Dox. Imaging continued for another 23 h to monitor changes in TDP-CTF levels. (**B**) Representative images of the induction of PABPN1 expression (green) and the subsequent reduction of TDP-CTF shown by heat map. (**C**) Quantification of PABPN1 protein levels after Dox induction. (**D**) Quantification of TDP-CTF protein levels over time. In the vehicle and GFP control groups, TDP-CTF steadily increased during the recording period, whereas the inducible PABPN1 expression caused a quick and sustained reduction of TDP-CTF levels. TDP-CTF protein levels from three independent experiments were normalized to the basal levels. Statistical analysis was performed with two-way repeat-measures ANOVA and Bonferroni's *post hoc* test (values at different time points versus value at 0 h, NS: not significant, $^{***}P < 0.001$, $n = 20$ per group). Graphs represent mean and SEM.

cytoplasmic foci) by ca. 65% within 24 h (35.6 ± 3.4%, $n = 20$) after co-expression GFP-PABPN1 was induced (Fig. 4B–D; Supplementary Material, Videos).

PABPN1 facilitates the clearance of pathological TDP-43 via the ubiquitin-proteasome mechanism

Previous studies on the mechanisms that govern the clearance of soluble and aggregated TDP-43 species demonstrate a role for both the UPS and autophagy (22). It has been suggested that hyperphosphorylation of TDP-43 may contribute to its accumulation in detergent-insoluble aggregates by modulating its oligomerization status (19,20) and protease resistance (21).

To determine the underlying mechanism by which PABPN1 reduced pathological TDP-43 protein, we first examined whether PABPN1 could alter the phosphorylation level of TDP-CTF. We transfected N2a cells with mCherry-TDP-CTF and GFP or GFP-PABPN1, and found that PABPN1 did not significantly change the relative phosphorylation level of TDP-CTF (Fig. 5A).

Western blot analysis showed that PABPN1 expression strongly reduced protein levels of TDP-CTF (32.8 ± 8.6), and also ALS-related mutant TDP-43 (TDP-43^{Q331K}: 47.0 ± 13.2%; TDP-43^{M337V}: 62.3 ± 5.1%; TDP-43^{A382T}: 49.9 ± 17.3%), but only weakly reduced TDP-43^{WT} levels (81.4 ± 1.9%) (Fig. 5B). Therefore, we decided to test whether PABPN1 increases the turnover of these proteins. We performed cycloheximide chase experiments to determine the half-life ($t_{1/2}$) of TDP-CTF and the temporal changes of relative TDP-CTF levels. PABPN1 co-expression reduced the half-life of TDP-CTF from 11.9 to 6.8 h (Fig. 5C1 and C2). We also observed that PABPN1 expression caused a steady decline in the relative TDP-CTF protein levels from 55 to 9.3% when compared with the GFP control over the 24-h time period (Fig. 5C4). The half-life and the relative level of endogenous TDP-43 were not affected (Fig. 5C3 and C5). The results show that PABPN1 expression enhances the turnover of truncated TDP-43 protein.

We used specific inhibitors to identify whether PABPN1 promoted the turnover of TDP-CTF via one of the two major protein degradation pathways: the UPS for soluble monomeric proteins and autophagy for soluble oligomeric proteins and insoluble large aggregates (22). Inhibiting autophagy by preventing the fusion between autophagosomes and lysosomes with bafilomycin A1 slightly prolonged the half-life of TDP-CTF but did not impair the PABPN1-dependent increase in turnover (GFP: $t_{1/2} = 12.4$ h; PABPN1: $t_{1/2} = 7.4$ h) (Fig. 5D1 and D2). The changes of the relative level of TDP-CTF resembled the results from the DMSO vehicle treatment (Fig. 5D4). However, inhibiting the proteolytic activity of 26S proteasome with MG-132 greatly decreased the degradation of TDP-CTF (GFP control: $t_{1/2} = 29.6$ h; GFP-PABPN1: $t_{1/2} = 30.5$ h) and completely abolished PABPN1's effect on TDP-CTF protein levels (Fig. 5E1 and E2). The relative level of TDP-CTF remained unchanged for the extended time period (Fig. 5E4). These results demonstrate that PABPN1 facilitates the removal of soluble monomeric TDP-CTF via the UPS.

We also observed a similar effect of PABPN1 expression on the protein turnover of mutant TDP-43^{M337V} and TDP-43^{WT}.

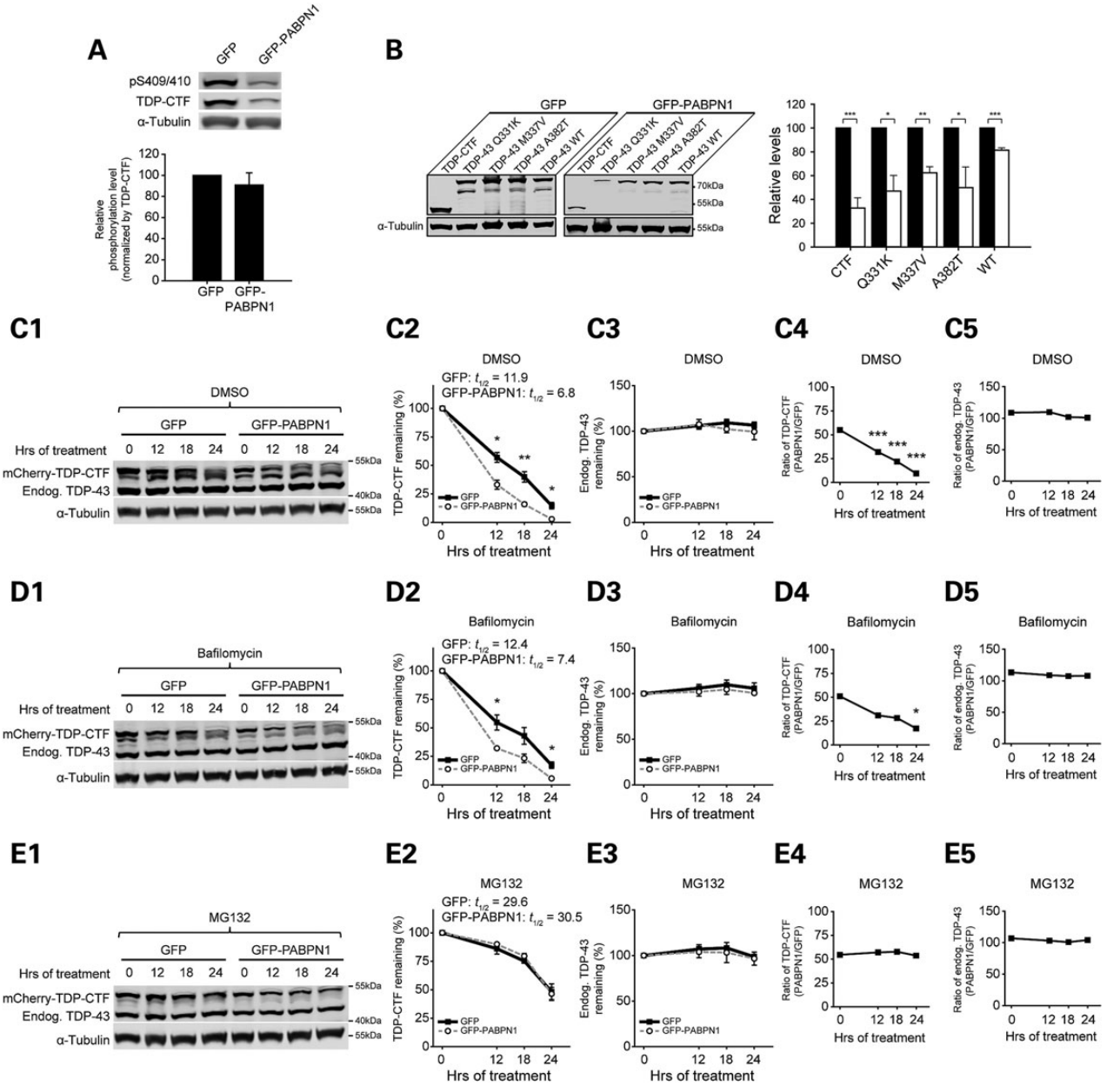

Figure 5. PABPN1 promotes TDP-CTF turnover through proteasomal degradation. (**A**) Quantification of phosphorylated TDP-CTF (normalized to total TDP-CTF protein levels). An antibody specific for phosphorylated Ser409/410 of TDP-43 was used. Statistical analysis was performed with Student's *t*-test. (**B**) PABPN1 expression reduces TDP-CTF, ALS-specific mutant TDP-43 (Q331K, M337V and A382T) and wild-type TDP-43 (WT). Statistical analysis with Student's *t*-test (*$P < 0.05$, **$P < 0.01$, ***$P < 0.001$, $n = 3$). (**C1–E1**) Cycloheximide chase assays to determine the half-life ($t_{1/2}$) and the relative protein levels of TDP-CTF. Representative western blots of lysates from N2a cells co-expressing mCherry-TDP-CTF with either GFP or GFP-PABPN1 are shown. Cells were treated with CHX (100 μM) together with DMSO vehicle control (C1), autophagy inhibitor Bafilomycin (100 nM) (D1) or proteasome inhibitor MG132 (10 μM) (E1) at the indicated time points. PABPN1 promoted TDP-CTF degradation only in the absence of proteasome inhibitors. (**C2–E2**) Quantification of TDP-CTF protein levels and half-life ($t_{1/2}$) after treatment with DMSO (C2), Bafilomycin (D2) or MG132 (E2). Protein levels were normalized to the values at 0 h and represented as the percentage of remaining protein. Statistical analysis is performed with Student's *t*-test (GFP-PABPN1 versus GFP, *$P < 0.05$, **$P < 0.01$, $n = 3$). (**C3–E3**) Quantification of endogenous TDP-43 protein levels and half-life ($t_{1/2}$). (**C4–E4**) Ratio of the relative TDP-CTF levels with PABPN1 versus GFP co-expression after treatment with DMSO (C4), Bafilomycin (D4) or MG132 (E4). TDP-CTF levels remained constant under conditions of proteasome inhibition. Statistical analysis was performed with one-way ANOVA and Bonferroni's *post hoc* test (values at different time points versus value at 0 h, *$P < 0.05$, ***$P < 0.001$, $n = 3$). (**C5–E5**) Ratio of the relative endogenous TDP-43 levels with PABPN1 versus GFP co-expression. Graphs represent mean and SEM.

Their half-life ($t_{1/2}$) changed from 28.6 to 16.7 h and 37.8 to 29.4 h, respectively (Fig. 6A1–A3), and there was a steady decline in the relative mutant TDP-43^{M337V} protein levels from 92.5 to 56.1% when compared with the GFP control over the 24-h time period (Fig. 6A4). Inhibiting autophagy by bafilomycin A1 prolonged the protein $t_{1/2}$ but did not abolish PABPN1's effects (Fig. 6B). However, inhibiting UPS activity compromised the PABPN1-specific rescue effect (Fig. 6C). These results confirm the suppression effect of PABPN1 on TDP-43 pathology, via a proteasome-dependent mechanism.

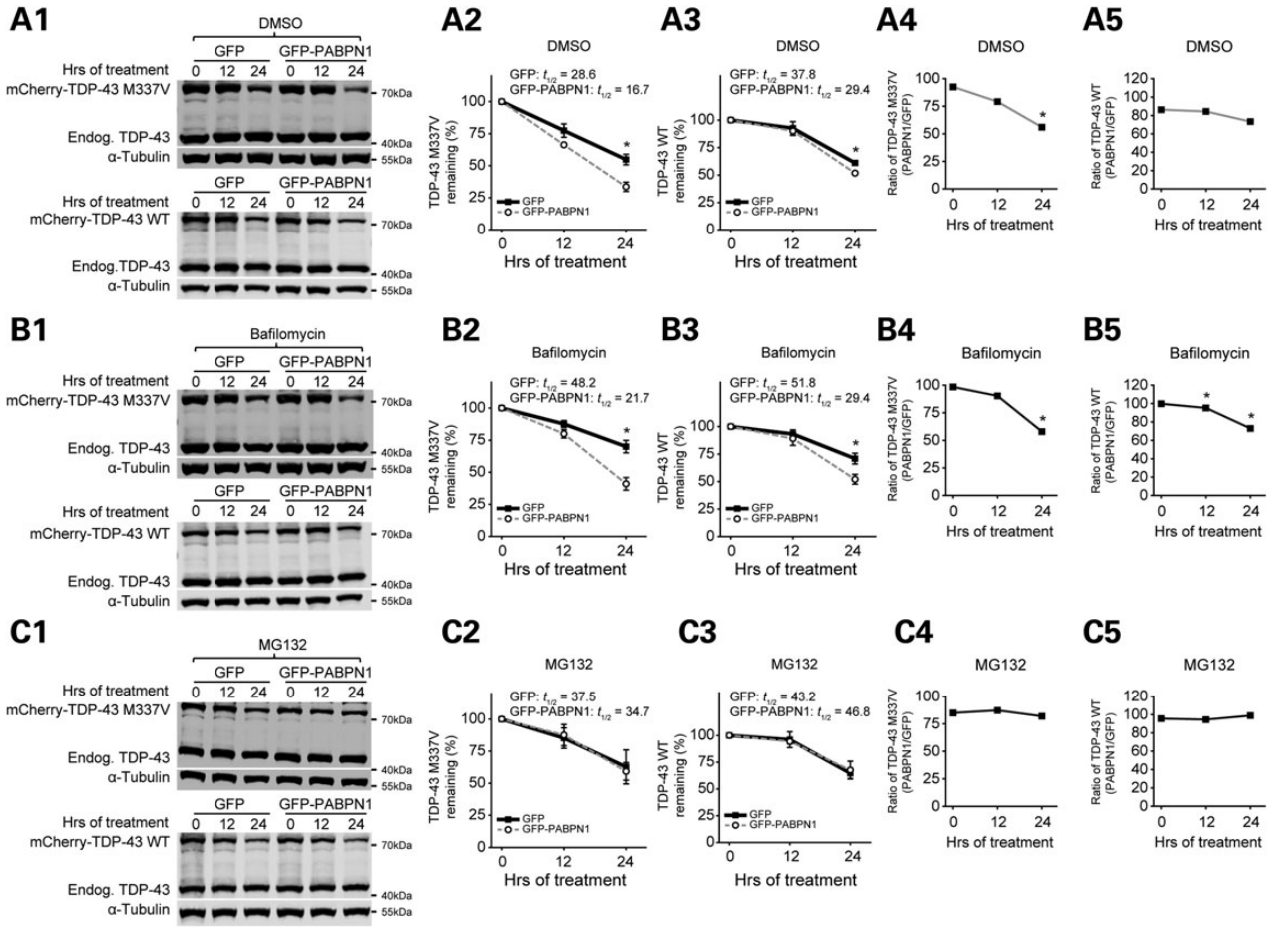

Figure 6. PABPN1 promotes mutant and wild-type TDP-43 turnover through proteasomal degradation. (**A1–C1**) Cycloheximide chase assays to determine the half-life ($t_{1/2}$) and the relative protein levels of mutant TDP-43 M337V and wild-type TDP-43 (WT). Representative western blots of lysates from N2a cells co-expressing mCherry-TDP-43 M337V or TDP-43 WT with either GFP or GFP-PABPN1 are shown. Cells were treated with CHX (100 μM) together with DMSO vehicle control (A1), autophagy inhibitor Bafilomycin (100 nM) (B1) or proteasome inhibitor MG132 (10 μM) (C1) at the indicated time points. PABPN1 promoted mutant and WT TDP-43 degradation only in the absence of proteasome inhibitors. (**A2–C2**) Quantification of TDP-43 M337V protein levels and half-life ($t_{1/2}$) after treatment with DMSO (A2), Bafilomycin (B2) or MG132 (C2). Protein levels were normalized to the values at 0 h and represented as the percentage of remaining protein. Statistical analysis is performed with Student's *t*-test (*GFP-PABPN1* versus *GFP*, $^{*}P < 0.05$, $n = 3$). (**A3–C3**) Quantification of TDP-43 WT protein levels and half-life ($t_{1/2}$). (**A4–C4**) Ratio of the relative TDP-43 M337V levels with PABPN1 versus GFP co-expression after treatment with DMSO (A3), Bafilomycin (B3) or MG132 (C3). TDP-43 M337V levels remained constant under conditions of proteasome inhibition. Statistical analysis was performed with one-way ANOVA and Bonferroni's *post hoc* test (values at different time points versus value at 0 h, $^{*}P < 0.05$, $^{***}P < 0.001$, $n = 3$). (**A5–C5**) Ratio of the relative TDP-43 WT levels with PABPN1 versus GFP co-expression. Graphs represent mean and SEM.

PABPN1 levels regulates nuclear localization of endogenous TDP-43

Cytoplasmic mislocalization of TDP-43 and its depletion from the nucleus is a prominent pathological feature in ALS. To investigate whether the expression of mutant TDP-43 or TDP-CTF leads to the mislocalization of endogenous full-length TDP-43, we transfected N2a cells with GFP-tagged TDP-43^{WT}, mutant TDP-43^{Q331K} and TDP-CTF. An antibody specific for the N-terminus of TDP-43 was used to determine the percentage of transfected cells that were positive for full-length TDP-43 in the cytoplasm and in the inclusions. The expression of TDP-CTF led to abundant cytoplasmic inclusions (61.0 ± 1.6%) and cytoplasmic mislocalization of endogenous TDP-43 (50.7 ± 2.9%). TDP-43^{WT} and TDP-43^{Q331K} predominantly localized to the nucleus with only ∼10% of cells exhibiting cytoplasmic TDP-43 inclusions. Mutant TDP-43^{Q331K} slightly increased the percentage of diffuse cytoplasmic mislocalization (32.8 ± 1.4%) when compared with TDP-43^{WT} (21.1 ± 1.2%) (Fig. 7A–C). These results suggested that the presence of cytoplasmic inclusions of pathologic TDP-43 fragments and ALS-specific mutations was detrimental to TDP-43 localization and caused the redistribution of full-length TDP-43 from the nucleus to the cytoplasm. This raised the question whether PABPN1 overexpression can reduce cytoplasmic mislocalization of TDP-43. The co-expressed PABPN1 significantly reduced the cytoplasmic inclusions (TDP-43^{WT}: 4.9 ± 1.2%; TDP-43^{Q331K}: 4.14 ± 0.6%; TDP-CTF: 14.0 ± 0.6%) and rescued TDP-43 nuclear localization in the cells expressing TDP-43^{WT}, TDP-43^{Q331K} and TDP-CTF (TDP-43^{WT}: 8.4 ± 0.6%; TDP-43^{Q331K}: 13.7 ± 1.7%; TDP-CTF: 18.2 ± 2.1%) (Fig. 7A–C). Similar results were also found in primary motor neurons, where PABPN1 expression reduced the number of cells with TDP-CTF aggregates by 54.8% and the number of cells with diffuse cytoplasmic TDP-43 mislocalization by 72.4% (Supplementary Material, Fig. S4). These results led us to investigate whether PABPN1 overexpression can rescue loss of normal TDP-43 from the nucleus. We performed nuclear-cytoplasmic fractionation experiments and western blot analyses with antibody specific for the N-terminus of TDP-43. Our

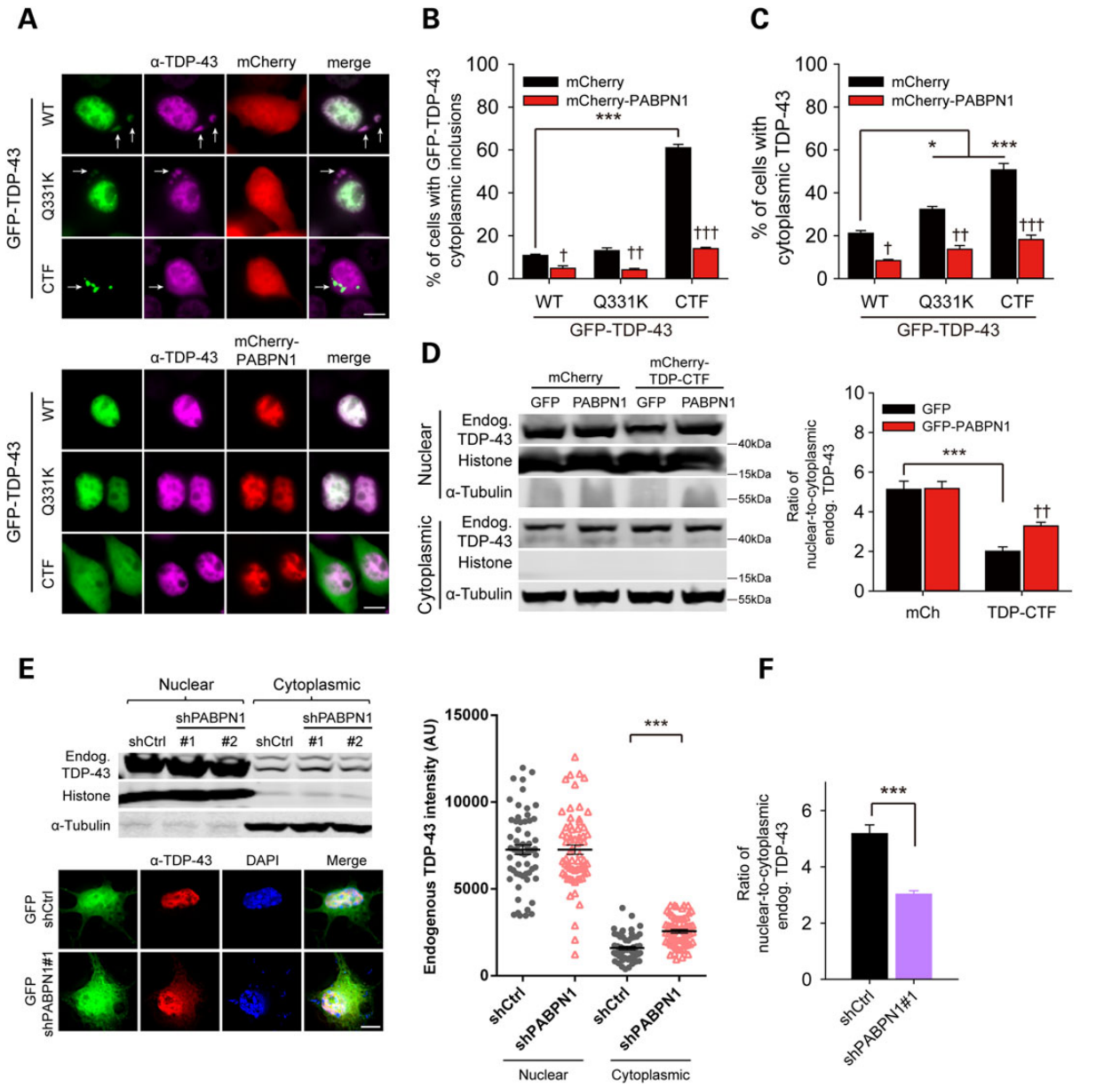

Figure 7. PABPN1 expression restores the nuclear localization of endogenous TDP-43. (**A**) Representative fluorescence microscopy images of N2a cells co-expressing GFP-tagged TDP-43^{WT}, TDP-43^{Q331K} or TDP-CTF, with either mCherry (top panels) or mCherry-PABPN1 (bottom panels). Full-length TDP-43 was stained with an antibody against an N-terminal region of TDP-43 (magenta). Mislocalized cytoplasmic TDP-43 is marked (white arrows). Scale bar: 10 μm. (**B** and **C**) Quantification of cells with GFP-TDP-43 cytoplasmic inclusions (B) and diffuse cytoplasmic TDP-43 staining (C). PABPN1 co-expression reduced the percentage of cells exhibiting cytoplasmic mislocalization and inclusions of full-length TDP-43. (**D**) Quantification of the nuclear-to-cytoplasmic ratio of endogenous TDP-43 in response to TDP-CTF co-expression with mCherry or mCherry-PABPN1. PABPN1 expression partially restored nuclear localization of endogenous TDP-43. Statistical analysis is performed with two-way ANOVA and Bonferroni's *post hoc* test ($^{*}P < 0.05$, $^{***}P < 0.001$; $^{\dagger}P < 0.05$, $^{\dagger\dagger}P < 0.01$, $^{\dagger\dagger\dagger}P < 0.001$, PABPN1 versus GFP or mCherry, $n = 3$). (**E** and **F**) Representative western blots and fluorescence microscopy images of endogenous TDP-43 in N2a cells (top panels) and primary motor neurons (bottom panels) after PABPN1 knockdown. Quantification of fluorescent intensity (AU) of nuclear and cytoplasmic TDP-43 (E) and nuclear-to-cytoplasmic ratio of endogenous TDP-43 in response to PABPN1 knockdown (F). Statistical analysis is performed with Student's *t*-test (three independent experiments, shCtrl versus shPABPN1#1, $^{***}P < 0.001$. shCtrl ($n = 59$), shPABPN1 ($n = 65$)). Graphs represent mean and SEM.

results demonstrated a shift of endogenous TDP-43 towards the cytoplasmic fraction upon TDP-CTF expression (Fig. 7D). Overexpression of PABPN1 partially reversed the pathologic changes to the ratio of nuclear-to-cytoplasmic endogenous TDP-43, demonstrating that PABPN1 overexpression can restore the proper nuclear localization of endogenous TDP-43. The knockdown of PABPN1, on the other hand, resulted in increased cytoplasmic localization of endogenous TDP-43 by 60.5% (Fig. 7E) and decreased the ratio of nuclear-to-cytoplasmic endogenous TDP-43 by 41.5% (Fig. 7F) in N2a cells and primary motor neurons.

PABPN1 overexpression rescues defects in SG formation caused by TDP-43 pathology

TDP-43 inclusions have been shown to colocalize with SG markers (e.g. TIA1, TIAR) in cultured cells and postmortem tissues from ALS patients (60). These studies suggest that genetic or

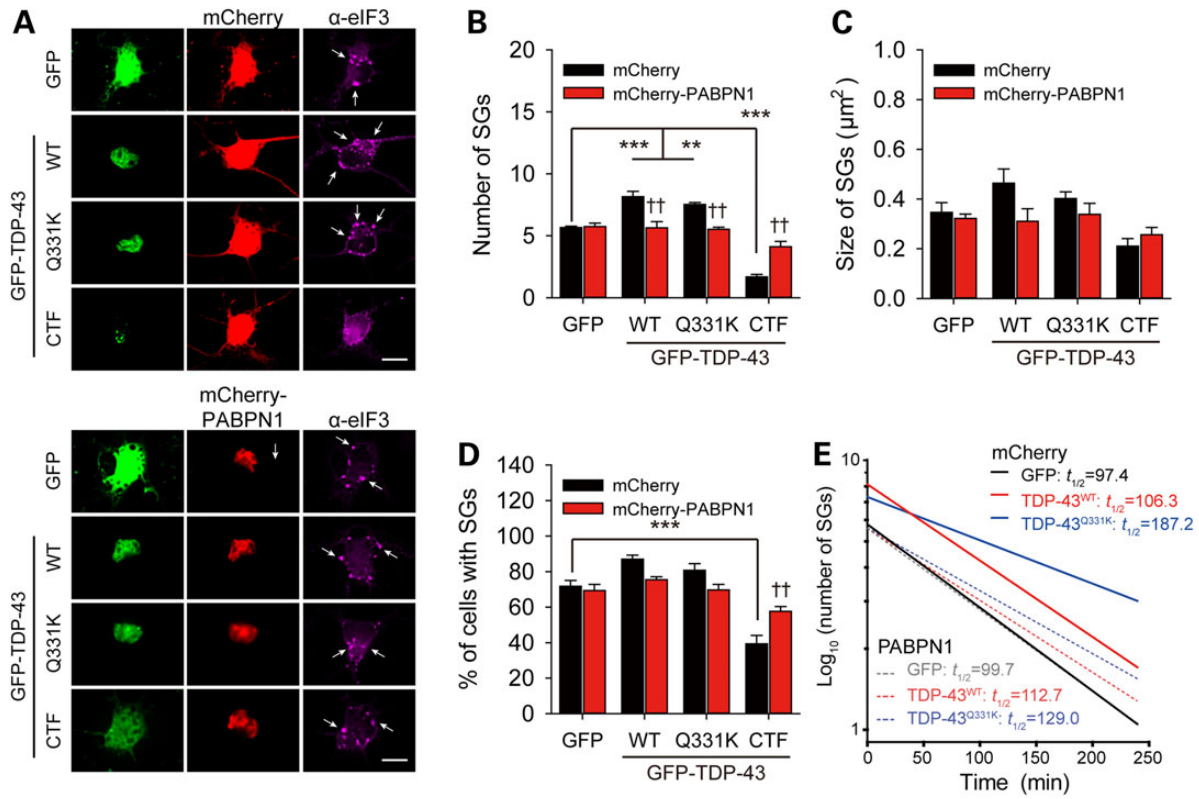

Figure 8. PABPN1 expression rescues SG formation defects caused by TDP-43 pathology. (**A**) Representative fluorescence microscopy images of eIF3-positive SGs (SGs) of primary motor neurons after exposure to 0.5 mM sodium arsenite for 24 h. Cells were co-transfected with GFP or GFP-tagged TDP-43^{WT}, TDP-43^{Q331K} or TDP-CTF with mCherry (top panels) or mCherry-PABPN1 (bottom panels). SGs were stained with an antibody against eIF3η (magenta). PABPN1 rescued TDP-CTF expression-mediated reduction of SG formation (white arrows). Scale bar: 10 μm. (**B–D**) Quantification of SG numbers (B) and sizes (C) and the percentage of cells with SGs (D). PABPN1 expression restored normal SG formation. Statistical analysis was performed with two-way ANOVA and Bonferroni's *post hoc* test (five independent experiments, $^{*}P < 0.05$, $^{**}P < 0.01$, $^{***}P < 0.001$; $^{\dagger}P < 0.05$, $^{\dagger\dagger}P < 0.01$, $^{\dagger\dagger\dagger}P < 0.001$, mCherry-PABPN1 versus mCherry, mCherry: GFP ($n = 65$), WT ($n = 86$), Q331K ($n = 76$), CTF ($n = 74$); mCherry-PABPN1: GFP ($n = 60$), WT ($n = 69$), Q331K ($n = 62$), CTF ($n = 73$)). Graphs represent mean and SEM. (**E**) Quantification of averaged half-time ($t_{1/2}$) of SG-disassembly in terms of SG numbers after the removal of oxidative stress (R0: GFP ($n = 47$), WT ($n = 49$), Q331K ($n = 57$); R2: GFP ($n = 38$), WT ($n = 51$), Q331K ($n = 51$); R4: GFP ($n = 48$), WT ($n = 51$), Q331K ($n = 46$)). PABPN1 expression rescued TDP-43-specific SG disassembly defects.

environmental factors leading to persistent SGs in the early stage of disease may not only interfere with RNA processing but also serve as precursors of pathological protein inclusions and trigger the irreversible formation of TDP-43 protein aggregates (61).

To investigate how TDP-43 pathology affects SG dynamics in primary motor neurons, we induced SGs by oxidative stress and quantified the SG assembly and disassembly in terms of SG formation and the half-life ($t_{1/2}$) of SG dissipation after removal of oxidative stress. Upon exposure to sodium arsenite (0.5 mM, 1 h), SG numbers differed greatly among the GFP control and the three TDP-43 constructs. TDP-43^{WT} and TDP-43^{Q331K} significantly increased SG numbers (GFP: 5.7 ± 0.1; TDP-43^{WT}: 8.2 ± 0.4; TDP-43^{Q331K}: 7.5 ± 0.2) (Fig. 8A and B), whereas TDP-CTF dramatically decreased the SG numbers (1.7 ± 0.2) and the percentage of SG-positive cells (GFP: 71.8 ± 3.3%; TDP-CTF: 39.3 ± 4.8%) (Fig. 8D). The SG size showed a similar trend (GFP: 0.35 ± 0.04; TDP-43^{WT}: 0.45 ± 0.06; TDP-43^{Q331K}: 0.40 ± 0.03; TDP-CTF: 0.21 ± 0.03) (Fig. 8C). Under normal conditions, SGs rapidly disassemble when the stressor is removed. However, TDP-43^{Q331K} expression caused SG persistence after stress resolution ($t_{1/2}$ = 187.2 min) as compared with GFP control and TDP-43^{WT} (GFP: $t_{1/2}$ = 97.4 min; TDP-43^{WT}: $t_{1/2}$ = 106.3 min) (Fig. 8E). These results show that the ALS-specific mutation in TDP-43^{Q331K} causes overactive SG assembly and slow SG disassembly. Previous studies reported that the mutant TDP-43 was more stable and resistant to degradation than wild-type TDP-43 (18). The failure in the dissipation of SGs could further increase the propensity of TDP-43 to form pathologic aggregates. To test whether PABPN1 can rescue TDP-43-specific impairment of SG dynamics, we co-expressed either mCherry or mCherry-PABPN1. Most strikingly, PABPN1 specifically restored SG formation in cells expressing TDP-CTF (Fig. 8A). Quantification of SG dynamics showed that PABPN1 expression alone did not perturb SG formation but rescued abnormal SG numbers (5.7 ± 0.3) and the percentage of SG-positive cells caused by pathological TDP-43 (Fig. 8A–D). Moreover, PABPN1 partially rescued the slower rate of SG disassembly caused by TDP-43^{Q331K} ($t_{1/2}$ = 129.0 min) (Fig. 8E). These results show that PABPN1 expression restores SG dynamics, a process that involves protein aggregation as part of its normal function, and may be closely linked to the disease process (14–16,61).

Discussion

Identifying regulators of TDP-43-induced pathogenesis could potentially provide therapeutic opportunities for a range of neurologic diseases. Evidence from genetic and neuropathological studies strongly implicates TDP-43 as a key player in the pathogenesis of primary TDP-43 proteinopathies in the ALS/FTLD-TDP clinicopathological spectrum (23,31). For other major neurodegenerative diseases where TDP-43 pathology is found at high rates, such as

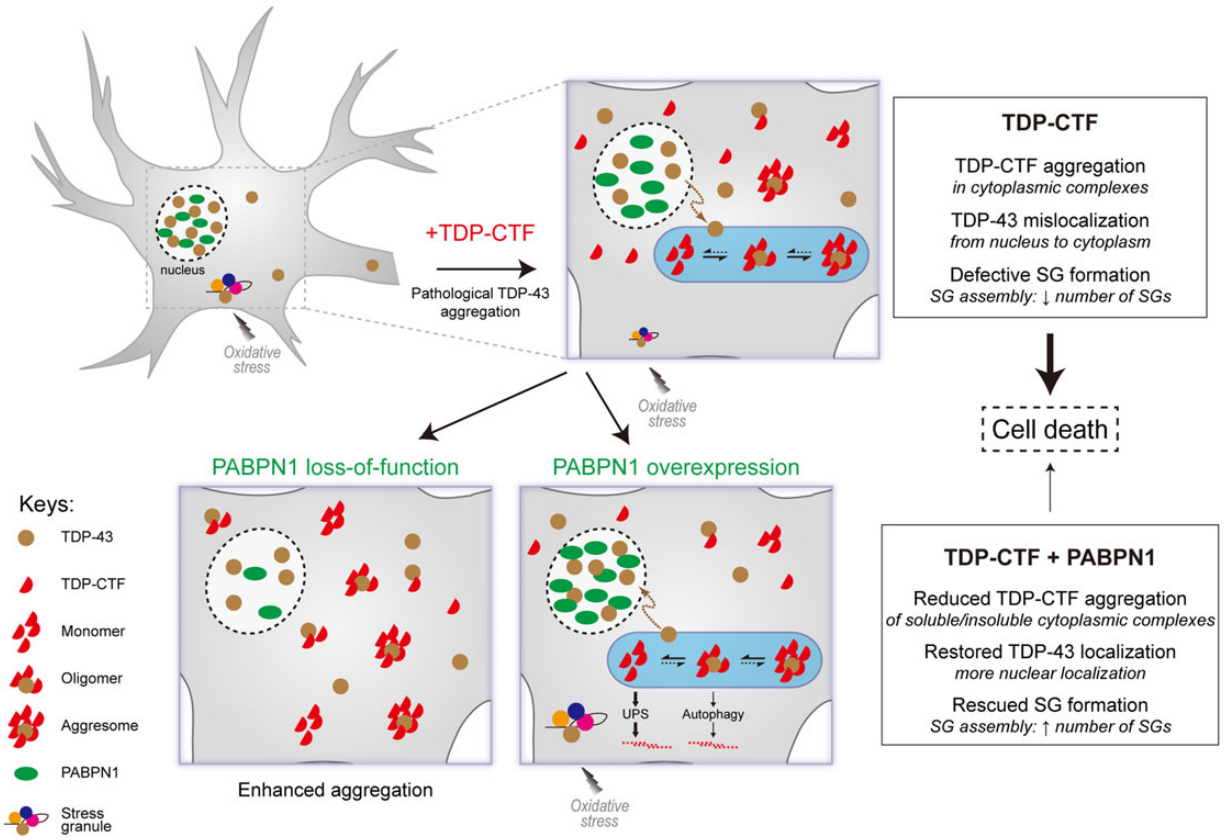

Figure 9. Model of PABPN1's effects on TDP-43 proteinopathy phenotypes. (Top) In healthy neurons, TDP-43 (brown) and PABPN1 (green) are primarily localized to the nucleus and TDP-43 is incorporated into SG under conditions of oxidative stress. Expression of pathological TDP-CTF (red) forms cytoplasmic aggregates, leads to mislocalization of full-length TDP-43 into the cytoplasm and compromises SG formation in response to oxidative stress. (Bottom left) PABPN1 loss-of-function exacerbates the accumulation of TDP-CTF and endogenous TDP-43 in the cytoplasm. (Bottom right) PABPN1 overexpression selectively promotes the degradation of TDP-CTF protein mainly via the UPS by driving the equilibrium towards soluble species and preventing the aggregation. The interaction of PABPN1 with TDP-43 directly or indirectly restores normal solubility and localization of TDP-43, and rescues SG assembly and disassembly defects under stress conditions. Taken together, these actions lead to the suppression of TDP-43-induced cell death.

AD, Huntington's disease, dementia with Lewy bodies and chronic traumatic encephalopathy, the extent of the contribution of TDP-43 proteotoxicity to the disease phenotype is currently not well understood (62).

In this study, we report PABPN1 as a novel interaction partner and potent suppressor of TDP-43 toxicity with unique properties. PABPN1 overexpression acts as a protective modifier in various cellular and animal models of TDP-43 proteinopathy concomitant with the selective degradation of pathological TDP-43 and the recovery of normal nuclear TDP-43 localization, whereas the loss of PABPN1 conversely serves as a toxic enhancer in the *in vivo* and *in vitro* models. Moreover, PABPN1 acts to rescue the TDP-43-induced dysregulation of SG dynamics, which has been considered a vicious cycle of TDP-43 pathology. Our study links the neuroprotective properties of PABPN1 to the acceleration of protein turnover of pathogenic TDP-43, which could potentially provide a new target to halt or even reverse the progression of TDP-43 pathology (Fig. 9).

Rescue of toxic gain of function of overexpressed TDP-43 variants in primary neurons, yeast and *Drosophila* models

TDP-43 pathology is characterized by two hallmarks: the accumulation of ubiquitinated, hyperphosphorylated and cleaved TDP-43 in mostly cytoplasmic aggregates, and the depletion of TDP-43 from the nucleus (2). Whether the pathogenesis of ALS is caused by a toxic gain-of-function of cytoplasmic mislocalized TDP-43 or by loss of its normal nuclear function is still under debate, but it appears likely that a combination of both contributes to the disease process (23,31). TDP-43 protein levels are tightly regulated (63), and increased or decreased levels may reduce cellular tolerance to intracellular or extracellular stress (64).

The gain-of-function hypothesis suggests that cytoplasmic TDP-43 mislocalization and its pathologic posttranslational modifications may directly acquire toxic properties, or trap mRNAs and proteins in insoluble aggregates (31). Therefore, most TDP-43 proteinopathy disease models are based on the overexpression of TDP-43 constructs. While modeling ALS pathology by transgenic overexpression of TDP-43 has not been entirely successful, these efforts have established that increasing wild-type or mutant TDP-43 levels by less than two-fold over endogenous levels is harmful (65).

To model this pathogenic mislocalization and aggregation in mammalian cells *in vitro*, several cellular models based on overexpression of C-terminal fragments of TDP-43 have been described (28). Most of these studies were performed in cell lines, but we and others have found that TDP-CTF forms hyperphosphorylated and ubiquitin-positive cytoplasmic aggregates in primary neurons and that disease-specific mutations increase the cytoplasmic localization of full-length TDP-43 (26,46).

Increasing toxicity is correlated with elevated TDP-43 levels and cytoplasmic TDP-43 mislocalization in cortical neurons (66). In this study we used wild-type hTDP-43 and several disease-specific mutations, as well as a C-terminal fragment of TDP-43 beginning at Arg208 that was found as a major component of pathologic inclusions in the brain of ALS and FTLD-TDP patients and recapitulates pathological features of TDP-43 proteinopathy when overexpressed (27,28). We found that overexpression of TDP-43 with disease-specific mutations enhanced the moderate toxicity of full-length TDP-43, and TDP-CTF caused the highest levels of cell death in primary cortical neurons (Fig. 2C and D). PABPN1 protein levels modulate TDP-43 toxicity, acting as a strong suppressor when overexpressed. Overexpression of PABPN1 alone did not show toxicity in primary neurons, well in agreement with data from transgenic mice overexpressing normal PABPN1 from a strong ubiquitous promoter with no obvious pathology (67).

TDP-43 proteinopathies and other neurodegenerative disorders characterized by the aggregation of proteins can be modeled in the budding yeast *Saccharomyces cerevisiae* (43). Not only TDP-43 but also FUS, α-synuclein and polyglutamate repeats are toxic and form cytoplasmic aggregates in yeast (68). Using suppressor screens, several functionally diverse yeast genes that can modulate TDP-43 toxicity have been identified (69–71). Pbp1 (poly(A)-binding protein (Pab1p)-binding Protein), and its ortholog Ataxin-2, were identified as a modulator of TDP-43 toxicity across multiple models, leading to the discovery of a significant association of Ataxin-2 intermediate-length polyQ tract expansions with ALS (71). Loss of the RNA lariat debranching enzyme *Dbr1* was able to antagonize the toxic effect of cytoplasmic TDP-43 aggregates in yeast and primary neurons (69). Accumulated intronic lariat RNAs may act as decoys that sequester TDP-43 away from binding to and disrupting functions of other RNAs. Another modifier of FUS- and TDP-43-mediated toxicity in yeast is ECM32, a component of the nonsense-mediated mRNA decay (NMD) surveillance mechanism that degrades mRNAs containing a premature termination codon (70). Overexpression of its human ortholog UPF1 protects primary neuronal cultures from TDP-43 cytotoxicity and preserves forelimb function in a rat model of TDP-43-induced motor paralysis, possibly by upregulating NMD (72). Expression of mutant variants of yeast Hsp104 was found to enhance the solubility of TDP-43 aggregates and suppress TDP-43 toxicity (73). In this study we employed a yeast model to find out whether PABPN1 expression can mitigate TDP-43 toxicity. While induced overexpression weakly inhibits growth in yeast, it acted as a strong suppressor of TDP-43 toxicity (Fig. 2A). Taken together with the direct interaction in the yeast two-hybrid tests, our results suggest a direct effect of PABPN1 on TDP-43 in yeast.

Several Drosophila models for TDP-43-associated ALS have provided evidence for both loss and gain-of-function hypotheses (74). Larvae expressing hTDP-43 in motor neurons are impaired in larval turning behavior, with disease-specific mutations having a more severe effect than wild-type TDP-43 (54,57). We evaluated the role of PABPN1 in regulating TDP-43 toxicity in vivo in a Drosophila model of ALS. Loss of PABPN1 function exacerbated TDP-43-specific neurodegeneration in both the adult retina and in larval motor neurons (Fig. 2G and H).

The C-terminus of PABPN1 contains a nonclassical proline-tyrosine nuclear localization signal, which is also present in FUS and other RNA-binding proteins and recognized by the nuclear import protein Transportin 1 (Trn1) (75). Although this signal is not essential for the nuclear import of human PABPN1 (76), larger deletions are required to confer nucleocytoplasmic ($PABPN1^{\Delta NLS18}$) or cytoplasmic ($PABPN1^{\Delta NLS50}$) localization (42). The $PABPN1^{\Delta NLS50}$ deletion mutant is still able to associate with TDP-43 in co-IPs (Fig. 1C) and even shows co-aggregation with TDP-CTF (Fig. 3A), although has weaker neuroprotective effects, which suggests that nuclear localization of PABPN1 is required for suppression of TDP-43 proteotoxicity. One possible model is that PABN1 interacts with monomeric and/or soluble forms of TDP-43 which are localized to the nucleus, thus preventing the formation of cytoplasmic aggregates of TDP-43.

TDP-43 toxicity may be caused by mislocalization of soluble cytoplasmic TDP-43 or by misfolding and/or aggregation into insoluble inclusions. The aberrant clusters of TDP-43, members of hnRNP family (e.g. hnRNP-A1, A2/B1), HuD, SG proteins (e.g. TIA-1, eIF3), SQSTM1/p62 and proteasome subunits suggested that cytoplasmic TDP-43 aggregation may disturb RNA and protein homeostasis (23). Alternatively, inclusion formation could protect cells from mislocalized cytoplasmic soluble TDP-43 protein (monomers or oligomers) by sequestering them into aggregates (77). To investigate how PABPN1 affects different populations of pathologic and normal TDP-43, we performed extensive analyses by fluorescence microscopy and western blot analysis of cell extracts. PABPN1 exhibits a remarkable specificity for pathologic forms of TDP-43. PABPN1 overexpression specifically reduced protein levels of both detergent-soluble and -insoluble forms of TDP-CTF (Fig. 3E), but it did not affect protein levels of endogenous full-length TDP-43. However, it caused a shift of endogenous TDP-43 from the insoluble to the soluble fraction, which suggested that PABPN1 may prevent the formation and/or facilitate the removal of existing TDP-CTF aggregates and also limit the co-aggregation of normal full-length TDP-43 (Fig. 3E). This finding was further supported by time-lapse live-cell imaging experiments to measure protein levels of TDP-CTF when PABPN1 expression was induced with a delay of 24 h. At this time point, cells exhibited high levels of TDP-CTF in the cytoplasm. PABPN1 but not GFP overexpression led to a rapid reduction of TDP-CTF protein levels throughout the cytoplasm. While live-cell imaging does not allow for discriminating soluble and insoluble TDP-CTF protein, we observed a reduction of both focal and more diffuse staining in the cytoplasm. This suggests that PABPN1 can cause the removal of existing aggregates either by facilitating their degradation or by preventing the formation of new aggregates. It remains to be investigated whether PABPN1 causes the release of TDP-43 associated proteins or RNAs that may be trapped by pathologic cytoplasmic TDP-43 aggregates.

Rescue of normal localization and solubility of endogenous TDP-43

The gain-of-function hypothesis suggests that cytoplasmic mislocalization and co-aggregation of TDP-43 may lead to its depletion from the nucleus, thus impairing its normal nuclear functions in regulating transcription and mRNA processing (29,31,78). While early-onset motor dysfunction in motor neuron-specific TDP-43 knockout mice may reflect an essential function of TDP-43 in development (79), knockout of TDP-43 in postnatal motor neurons led to an age-dependent progressive motor dysfunction accompanied by neuropathological alterations typical for ALS, including axonal degenerations preceding atrophy of motor neurons (80,81). A specific vulnerability of motor neurons to low TDP-43 levels is supported by transgenic CNS-specific TDP-43 knockdown mice that exhibit age-dependent neurological symptoms, including muscle weakness and paralysis, concomitant with degeneration of spinal motor neurons (30).

In cell lines, the overexpression of different TDP-CTF variants leads to the recruitment of endogenous TDP-43 into the cytoplasm

(17,82,83). Consistent with a loss-of-nuclear function phenotype, the expression of TDP-CTF constructs can affect the TDP-43-dependent regulation of cystic fibrosis transmembrane conductance regulator alternative splicing (17,83,84). When we overexpressed TDP-CTF in N2a cells, we also observed reduced nuclear levels of endogenous TDP-43 (Fig. 7D). These results suggest that the presence of TDP-CTF, exhibiting abundant cytoplasmic aggregates, drives endogenous TDP-43 from the nucleus into the cytoplasm, which may disturb neuronal function via a loss-of-function mechanism. Therefore, removal of pathogenic TDP-43 concurrent with restoring normal levels of nuclear TDP-43 may be required for a complete rescue of TDP-43 proteinopathy models. Importantly, we found that PABPN1 overexpression not only failed to disturb protein levels of endogenous TDP-43 but also rescued its nuclear localization and solubility (Figs. 3E and 7D). This effect is likely due to the reduction of TDP-CTF protein levels and cytoplasmic aggregates, which allows the release of trapped TDP-43 and the recovery of its nuclear localization and function.

Interestingly, the neuromuscular disease OPMD, caused by polyalanine expanded mutant PABPN1, is characterized by TDP-43-positive aggregates in affected muscle cells (36). While initially toxic gain-of-function models have been proposed (85), low levels of PABPN1 observed in skeletal muscle and a loss of normal PABPN1 function may contribute to the muscle-specific pathology in OPMD (35,86,87). Since we observed an increase in TDP-CTF protein levels (Fig. 3C) and cytoplasmic redistribution of endogenous TDP-43 (Fig. 7E and F) after knockdown of PABPN1, it is tempting to speculate that low levels of functional PABPN1 could contribute to the accumulation and mislocalization of TDP-43 in OPMD.

Rescue of SG formation by PABPN1

SG formation involves protein accumulation as a normal mechanism and might play an important role in the pathogenesis of TDP-43 proteinopathies, by acting as a seed for pathological inclusions and by sequestering RNAs and associated proteins (16,61). TDP-43 has been found colocalized with several SG proteins (e.g. TIA-1, TIAR and eIF3) in cultured cells and brain tissues from ALS and FTLD-TDP patients, which hypothetically links the prolonged misregulation of SG dynamics to the cytoplasmic aggregation formation (15). However, whether the genetic mutation or protein aggregation could conversely interfere with the SG formation is poorly understood. TDP-43 modulates SG dynamics through the regulation of the essential SG nucleators TIA-1 and G3BP (88). Q331K and Q343R mutation were found to enhance SG formation in BE-M17 cells (13), suggesting that the aggregation-prone and degradation-resistant properties of mutant TDP-43 may contribute to the dysregulation of SG dynamics.

In the present study, we demonstrated that mutant or aggregated TDP-43 impeded normal SG dynamics in primary motor neurons under conditions of oxidative stress (Fig. 8). We observed the overactive SG formation in cells overexpressing wild-type TDP-43 or mutant Q331K but loss of SGs in TDP-CTF expressing neurons. Moreover, we also found the prolonged SG disassembly in TDP-43^{Q331K} instead of TDP-43^{WT} (Fig. 8). While TDP-CTF lacks the RNA-binding domains necessary for SG association (60), its aggregation in the cytoplasm may potentially interfere with normal SG formation by trapping essential SG components into its aggregates, which may render neurons more vulnerable to sublethal stress condition. The rescue effect of PABPN1 on SG dynamics in TDP-43 pathology is likely due to enhancing the turnover of pathogenic TDP-43 and restoring solubility and localization of normal TDP-43 protein.

How does PABPN1 regulate levels of pathologic TDP-43?

Two principal pathways of protein degradation have been described as complementary neuroprotective mechanisms, the UPS characterized by the degradation of polyubiquitinated substrates via the proteasome, and the autophagy pathway, typically targeting larger aggregates for degradation in lysosomes (89). Previous studies have shown that induction of autophagy and proteasome activity both facilitate TDP-43 clearance and ameliorated toxicity (66,90,91). Several studies have reported distinct roles for protein degradation pathways in the clearance of pathological TDP-43 proteins (22,92). As pathological TDP-43 exists in various forms, the UPS appears to preferentially degrade soluble monomeric TDP-43, whereas autophagy removes oligomeric and aggregated TDP-43.

Our data show that inhibition of proteasomes but not autophagy completely blocked PABPN1-dependent degradation of TDP-CTF and mutant TDP-43 (Figs 5 and 6). Although we cannot exclude the contribution of autophagy system to the protein degradation of detergent-insoluble large aggregates, the UPS appears to be more important to degrade pathological TDP-43 isoforms in the presence of PABPN1. Our results demonstrate that PABPN1 enhanced the protein turnover of exogenously expressed wild-type TDP-43, mutant TDP-43 and TDP-CTF preferentially through the UPS degradation pathway by driving the equilibrium towards small soluble species and preventing the formation of macroaggregates (Fig. 9).

Further studies are needed to establish the exact mechanism how PABPN1 specifically targets pathologic TDP-43. The observation that the C-terminal NLS of PABPN1 is required for this activity suggests that it may directly affect the localization of TDP-43, perhaps by facilitating its nuclear import. Alternatively, PABPN1 may have a direct effect on the degradation of TDP-43 via regulating UPS pathways. In addition, there are several functional links between poly(A)-binding proteins and TDP-43 toxicity. In yeast, Pbp1 enhances TDP-43 toxicity. Pbp1 interacts with Pab1 to regulate mRNA polyadenylation and is involved in SG assembly, and the same has been found for their mammalian homologs Ataxin-2 and PABPC1 (71). In a *Drosophila* model of ALS, dPABP expression exacerbates TDP-43 toxicity and PABPC1 was found to be mislocalized in cytoplasmic accumulations in ALS patient motor neurons (58). This is further supported by our finding that PABPC1 overexpression had an opposite effect of PABPN1 and increased TDP-CTF protein levels (Fig. 3D).

In conclusion, whether TDP-43 proteinopathy is due to gain- or loss-of-function mechanisms or a combination of both, our results suggest that the specific removal of pathologic TDP-43 protein by modulating PABPN1 protein levels can rescue various phenotypes caused by TDP-43 toxicity, and restore normal localization of TDP-43 across several *in vitro* and *in vivo* disease models (Fig. 9). A better understanding of pathways that regulate TDP-43 proteinopathy may form the basis of novel strategies for therapeutic intervention in ALS, FTLD-TDP and other neurodegenerative diseases.

Materials and Methods

Yeast two-hybrid assay

Full-length murine TDP-43 was cloned into as fusion with the GAL4 DNA-binding domain (pGBKT7, Clontech), transformed into the yeast strain AH109 (Mat a) and used as a bait in a yeast two-hybrid screen with the pretransformed 17-day murine embryo cDNA library (Clontech) in strain Y187 (MATα). A total of 2.91×10^7 diploid yeast cells containing both bait and prey plasmids were screened according to the Matchmaker 3 protocol

(Clontech) and a C-terminal fragment of PABPN1 was identified as a potential new interaction partner and further analyzed. To confirm the interaction of full-length proteins, full-length hTDP-43 and hPABPN1 cDNA were cloned as fusions with the GAL4 DNA-binding domain (pGBKT7, Clontech) and the GAL4 activation domain (pGADT7, Clontech). Plasmids were transformed into the *S. cerevisiae* GAL4 reporter strain AH109 (Clontech) using the PEG/lithium acetate method according to the Matchmaker protocol (Clontech). Transformants were streaked out onto selective plates (SD/-Ade/-His/-Leu/-Trp; +20 μg/mL X-α-Gal) to assess growth and to visualize blue colonies positive for yeast two-hybrid interaction.

Yeast spotting assays

Expression cassettes for hTDP-43-YFP (Addgene plasmid 27447) (44) and hPABPN1 fused to monomeric Cerulean fluorescent protein (Addgene plasmid 14417) (93) under control of the galactose-inducible GAL1 promoter were cloned into 2μ high-copy plasmids pRS425 (LEU2) and pRS426 (URA3). As control plasmids, pRS425-YFP and pRS426-mCerulean were used. Yeast cells were co-transformed with plasmids using the PEG/lithium acetate method and plated onto synthetic drop out media (SD/-Leu/-Ura; +2% glucose). For spotting assay, cells were grown overnight at 30°C. The cell numbers were determined by OD_{600}, serially diluted by a factor of 10 (1, 0.1, 0.01 and 0.001), and spotted onto solid synthetic drop out media (SD/-Leu/-Ura; + 2% glucose or + 2% galactose). Cells were grown at 30°C for 2–3 days.

Drosophila genetics

All *Drosophila* stocks and crosses were kept on standard yeast/cornmeal/molasses food at 25°C. Gal4 drivers used in the present study include the eye-specific GMR Gal4 R13 and the motor neuron driver D42 Gal4. Transgenic lines of GMR Gal4 wild-type hTDP-43 (hwt), D169G (hD169G), A315T (hA315T), ΔRRM and G298S (hG298S) were generated as described (54). For genetic interactions, stock FBst0038390 with a loss-of-function allele of Pabp2 was used (Pabp2 [55]/CyO, P(w[+mC] = ActGFP)cJMR1) (56). Larval turning assays were performed as previously described (54,57). Briefly, third instar wandering larvae were placed and acclimated on a plate at room temperature. The crawling larvae were turned onto their backs (ventral side up), and the amount of time each larva took to turn back (dorsal side up) and continued the forward movement was recorded. Thirty to 40 larvae were used per genotype.

Primary neuron culture and transfection

Primary motor neurons from spinal cords of mice embryos at Day 13.5 (E13.5) were isolated and cultured for 2 days and transfected by magnetofection as previously described (94,95). Primary cortical neurons were isolated from cerebral cortices of mice embryos at Day 17 (E17). Neurons grown on coverslips were inverted onto the dishes in the presence of a glial feeder layer in conditioned medium (Neurobasal medium, 1% Glutamax and 2% B-27 supplements), and cultured for 4 days prior to transfection with Lipofectamine 2000 reagent. Enhanced blue fluorescent protein 2 (BFP), or monomeric green (GFP) or red (mCherry) fluorescent proteins were fused to hwt TDP-43 ($TDP\text{-}43^{WT}$), mutant TDP-43 ($TDP\text{-}43^{Q331K}$, $TDP\text{-}43^{M337V}$ and $TDP\text{-}43^{A382T}$) and a C-terminal fragment of TDP-43 (aa 208–414, TDP-CTF) as described (46). GFP-PABPN1 was a generous gift by the Rouleau lab (96). BFP, GFP or mCherry fluorescent proteins were also fused to human full-length PABPN1 and truncation mutations of PABPN1 ($PABPN1^{\Delta NLS18}$ and $PABPN1^{\Delta NLS50}$). A flexible linker [(SGGG)3] was inserted between all the fusion partners to facilitate correct protein folding. The pGIPZ shRNA vectors for targeting PABPN1 sequences (shPABPN1#1, V3LHS_646409; shPABPN1#2, V3LHS_644004) and a nonsilencing control (shCtrl, RHS4346) obtained from Open Biosystems were used for PABPN1 knockdown experiments. mCherry-tagged hnRNPA3 and HA-tagged Htt Exon1-150Q (a gift from Dr Xiao-Jiang Li) (59) were transfected into primary cortical neurons. GFP-PABPN1 and GFP were cloned behind the doxycycline-inducible Tet-On promoter in the expression vector pTRIPZ (Open Biosystems), and transfected into primary cortical neurons for time-lapse live-cell imaging.

Mammalian cell culture and transfection

N2a neuroblastoma cells were cultured in DMEM medium (Invitrogen) containing 10% FBS (Hyclone) and 1% PenStrep (Sigma), and transfected with the Turbofect reagent (Fermentas) following manufacturer's instructions. Cells were fixed 48-h after transfection.

Cell staining and image acquisition and analysis

For the overexpression experiments, primary neurons were fixed 1 day and N2a cells were fixed 2 days after transfection. For shRNA-mediated knockdown experiment, cells were fixed 4 days after transfection. Transfected cells expressing shRNA constructs, identified by GFP expression, showed a significant reduction in endogenous PABPN1 protein levels. Cells were fixed with 4% paraformaldehyde in PBS for 15 min at room temperature, permeabilized with 0.2% Triton X-100/PBS for 5 min and blocked with 5% BSA for 45 min. Primary antibodies were incubated overnight at 4°C. Cy2-, Cy3- or Cy5-conjugated secondary antibodies (Jackson ImmunoResearch) were incubated for 1 h at room temperature. Fluorescent imaging was acquired with an epifluorescent microscope (Ti, Nikon) using a ×60 objective (1.4 NA). Within each experiment, all groups were imaged with the same acquisition settings. Z-series (5–10 sections, 0.15 μm steps) were acquired. Image stacks were deconvolved using a 3-D blind constrained iterative algorithm (AutoQuant, Media Cybernetics) and analyzed using ImageJ software (National Institutes of Health) (97). For the quantification of SGs, a cell body region of a transfected cell was selected and all granules above a pre-determined threshold level were quantified using the Particle Analysis function of ImageJ software. Primary antibodies were used according to the Supplementary Material, Table.

Cell death assay

Cell death of primary cortical neurons was assessed by the uptake of membrane-impermeant ethidium homodimer-1 (EthD-I, Biotium). EthD-I labels nucleic acids of membrane-compromised dying/dead cells and reveals strong red fluorescence in nucleus (excitation/emission maxima ~528/617 nm). After transfection, 2 μM EthD-I was added to culture medium for 1 h at 37°C. Cell death was determined by visually counting under an epifluorescent microscope. Rate of cell death in % = number of transfected cells with red fluorescence in nucleus/number of transfected cells × 100%.

Co-immunoprecipitation of FLAG-tagged constructs from mammalian cells

N2a cells were co-transfected with FLAG-TDP-43, and GFP or GFP-tagged PABPN1, $PABPN1^{\Delta NLS18}$ or $PABPN1^{\Delta NLS50}$ using Turbofect

reagent (Fermentas). Two days after transfection, cells were resuspended in lysis buffer (50 mM Tris–HCl, pH 7.5, 150 mM NaCl, 1 mM EDTA, 1% Triton X-100, Roche complete protease inhibitor cocktail) and centrifuged for 20 min at 20 000 × *g*. RNaseA was added at 37°C for 30 min. A small aliquot of the supernatant was collected as input extract, and the rest was used for co-immunoprecipitation. The supernatant was incubated with anti-FLAG (Sigma-Aldrich) agarose beads for 2 h at 4°C with rotation. Beads were washed five times with lysis buffer. Input extract and anti-FLAG immunoprecipitates were boiled with Laemmli buffer and used for western blot analysis. Primary antibodies were used according to Supplementary Material, Table.

Co-immunoprecipitation of endogenous protein from mouse brain tissue

Brains from E13.5 mouse embryos were flash frozen in liquid nitrogen immediately following dissection and kept at −80° until needed. Brains were homogenized with a dounce homogenizer on ice in 1 ml of lysis buffer, then sonicated and spun down at 20 000 × *g* for 15 min. A small aliquot of input from the supernatant was set aside, and the rest was used for co-immunoprecipitation. Immunoprecipitation of PABNP1 was performed with rabbit monoclonal anti-PABPN1 (Epitomics) and Protein A-agarose beads (Calbiochem) according to manufacturer's instructions. Normal rabbit serum (Millipore) was used as a control. Beads were washed five times with lysis buffer and boiled in Laemmli sample buffer. Samples were separated on a 10% SDS–PAGE gel, blotted onto nitrocellulose membranes and blocked with Odyssey blocking buffer (LiCor). Primary antibodies were used according to the Supplementary Material, Table.

Histidine pulldown assay

N2a cells were co-transfected with histidine-tagged mCherry-TDP-CTF, and GFP or GFP-tagged PABPN1. Cells were resuspended in lysis buffer (50 mM Tris–HCl, 150 mM NaCl, 1 mM EGTA, 1% NP-40, 0.25% sodium deoxycholate, 1 mM Na_3VO_4 and Roche complete protease inhibitor cocktail) and centrifuged for 20 min at 20 000 × *g*. The supernatant was incubated with Nickel-resin (His60 Ni Superflow Resin, Clontech) for 2 h at 4°C with rotation. The mixture was washed with lysis buffer and boiled with Laemmli buffer to elute bound proteins for western blot analysis.

Protein extract, subcellular fractionation and western blots

For protein extract experiment, N2a cells were co-transfected with mCherry or mCherry-TDP-CTF, and GFP or GFP-tagged PABPN1, PABPN1$^{\Delta NLS18}$, PABPN1$^{\Delta NLS50}$ or PABPC1 using Turbofect reagent (Fermentas). Cells were lysed in RIPA buffer (50 mM Tris, pH 8.0, 150 mM NaCl, 1% NP-40, 0.1% SDS, 0.5% sodium deoxycholate and Roche complete protease inhibitor cocktail). After 20 min incubation on ice, cells were sonicated briefly and centrifuged at 20 000 × *g* for 15 min. The supernatant was collected as the whole-cell lysate. For the protein detergent solubility assay, Neuro2a cells were resuspended in lysis buffer (50 mM Tris–HCl, pH 8.0, 150 mM NaCl, 1 mM EDTA, 1% Triton X-100, Roche complete protease inhibitor cocktail). After 20 min incubation on ice, cells were sonicated briefly and centrifuged at 20 000 × g for 15 min. The supernatant was collected as the detergent-soluble fraction and the insoluble pellet was recovered in urea buffer (8 M urea, 50 mM Tris–HCl, pH 8.0, Roche complete protease inhibitor cocktail). Following sonication and max-speed centrifugation, the supernatant was collected as the detergent-insoluble fraction. For the nuclear and cytoplasmic fractionation, N2a cells were lysed in hypotonic buffer (10 mM HEPES, pH 7.9, 20 mM KCl, 0.1 mM EGTA, 1 mM DTT and Roche complete protease inhibitor cocktail), left on ice for 15 min, 0.1% NP-40 was added for another 5 min and lysates were centrifuged at 15 600 × *g* for 10 min at 4°C. The supernatant was collected as cytoplasmic fraction, and the pellet containing the nuclei was suspended in high salt buffer (20 mM HEPES, pH 7.9, 0.4 M NaCl, 0.1 mM EDTA, 0.1 mM EGTA, 1 mM DTT, 5% glycerol and Roche complete protease inhibitor cocktail). The suspension was incubated on ice for 30 min, sonicated once and centrifuged at 15 600 × *g* for 10 min at 4°C. The supernatant was saved as the nuclear fraction. For western blot analysis, the samples were boiled in Laemmli sample buffer for 5 min and separated by 10% SDS–PAGE. mCherry-TDP-CTF, full-length TDP-43, PABPN1 and α-tubulin were detected by corresponding primary antibodies. Specific secondary antibodies conjugated with infrared dyes (Li-Cor) were used for detection on an Odyssey scanner (Li-Cor). Primary antibodies were used according to Supplementary Material, Table.

Cycloheximide chase assay

N2a cells were co-transfected with mCherry-TDP-CTF, and GFP or GFP-tagged PABPN1. Twenty-four hours after transfection, cells were treated with 100 μM cycloheximide (Sigma-Aldrich). At each indicated time point, cells were also treated with either vehicle (DMSO), 100 nM Bafilomycin (Cayman Chemical), or 10 μM MG132 (Sigma-Aldrich), and incubated from 0 to 24 h. Cells were lysed in RIPA buffer with Roche complete protease inhibitor cocktail. After 20 min incubation on ice, cells were sonicated briefly and centrifuged at 20 000 × *g* for 15 min. The protein concentration was determined using Bradford protein assay. Western blotting was performed as previously described. Antibodies were used to against mCherry-TDP-CTF, endogenous TDP-43 and α-Tubulin. The protein levels were normalized to the values at 0 h and represented as the percentage of remaining protein. The temporal changes of relative protein levels were determined by the ratio change of mCherry-TDP-CTF or endogenous TDP-43 between the PABPN1 and GFP coexpression at each indicated time point.

Time-lapse live-cell imaging

Two to three thousands of primary cortical neurons were plated in a glass bottom culture dish (MatTek Corporation, 35 mm petri dish, 14 mm microwell) and cultured in conditioned medium for 4 days. To evaluate the dynamics of TDP-CTF, neurons were co-transfected with constitutive CMV promoter-driven mCherry-TDP-CTF and inducible Tet-On promoter-driven GFP or GFP-PABPN1 plasmids using Lipofectamine 2000 reagent for 24 h. We monitored neurons by time-lapse microscopy on a Nikon BioStation IM (Nikon Instruments Inc., Melville, NY, USA) using an 80 × 0.8 NA objective. Neurons were maintained at 37°C and 5% CO_2 in the chamber throughout the experiment. During the first hour of the experiment, the mean fluorescence intensity of TDP-CTF in cell body was measured as the basic protein level (100%). Then expression of GFP or GFP-PABPN1 under control of the Tet-On promoter was induced with doxycycline (Dox) (0.5 μg/ml) (Clontech) for the next 23 h. DMSO was used as vehicle control. Each neuron was captured every 10 min over 24 h with phase contrast and fluorescence imaging in the red and green channels. The intensity measurements of mCherry-TDP-CTF were normalized to th1be basic protein level following treatment and plotted as the change of relative mCherry-TDP-CTF.

Stress granule formation assay

Primary motor neurons were co-transfected via magnetofection as described (94) with mCherry or mCherry-PABPN1, and GFP or GFP-tagged TDP-43^{WT}, TDP-43^{Q331K} or TDP-CTF for 24 h and then exposed to 0.5 mM sodium arsenite for 1 h to induce formation of SGs. Neurons were fixed and SGs were detected by goat anti-eIF3η (N-20, Santa Cruz Biotechnology; 1 : 200) antibodies. The number and size of SGs and the percentage of cells with SGs were measured using ImageJ software. To quantify the disassembly of SGs after the removal of sodium arsenite, the number of SGs was measured after 0, 2 or 4 h.

Statistical analyses

Data from different experiments were analyzed by mean value analysis (Student's *t* test) or analysis of variance (one- or two-way ANOVA) using GraphPad Prism Software. Differences were considered significant when $P < 0.05$. All values are mean and SEM.

Supplementary Material

Supplementary Material is available at *HMG* online.

Acknowledgements

We thank Dr Gary Bassell, Dr Christina Gross and Dr Claudia Fallini for valuable comments, and Dr Xiao-Jiang Li and Dr Guy A. Rouleau for plasmids. We thank Lian Li and Dr Eric B. Dammer for technical assistance.

Conflict of Interest statement. None declared.

Funding

This work was supported by the Muscular Dystrophy Association and ALS Association to W.R. and NIH NS078429 to D.C.Z.

References

1. Lagier-Tourenne, C. and Cleveland, D.W. (2009) Rethinking ALS: the FUS about TDP-43. *Cell*, **136**, 1001–1004.
2. Neumann, M., Sampathu, D.M., Kwong, L.K., Truax, A.C., Micsenyi, M.C., Chou, T.T., Bruce, J., Schuck, T., Grossman, M., Clark, C.M. *et al*. (2006) Ubiquitinated TDP-43 in frontotemporal lobar degeneration and amyotrophic lateral sclerosis. *Science*, **314**, 130–133.
3. Arai, T., Hasegawa, M., Akiyama, H., Ikeda, K., Nonaka, T., Mori, H., Mann, D., Tsuchiya, K., Yoshida, M., Hashizume, Y. *et al*. (2006) TDP-43 is a component of ubiquitin-positive tau-negative inclusions in frontotemporal lobar degeneration and amyotrophic lateral sclerosis. *Biochem. Biophys. Res. Commun.*, **351**, 602–611.
4. Mackenzie, I.R. (2007) The neuropathology of FTD associated With ALS. *Alzheimer. Dis. Assoc. Disord.*, **21**, S44–S49.
5. Mackenzie, I.R., Rademakers, R. and Neumann, M. (2010) TDP-43 and FUS in amyotrophic lateral sclerosis and frontotemporal dementia. *Lancet. Neurol.*, **9**, 995–1007.
6. Chen-Plotkin, A.S., Lee, V.M. and Trojanowski, J.Q. (2010) TAR DNA-binding protein 43 in neurodegenerative disease. *Nat. Rev. Neurol.*, **6**, 211–220.
7. Lagier-Tourenne, C., Polymenidou, M. and Cleveland, D.W. (2010) TDP-43 and FUS/TLS: emerging roles in RNA processing and neurodegeneration. *Hum. Mol. Genet.*, **19**, R46–R64.
8. Buratti, E. and Baralle, F.E. (2001) Characterization and functional implications of the RNA binding properties of nuclear factor TDP-43, a novel splicing regulator of CFTR exon 9. *J. Biol. Chem.*, **276**, 36337–36343.
9. Cushman, M., Johnson, B.S., King, O.D., Gitler, A.D. and Shorter, J. (2010) Prion-like disorders: blurring the divide between transmissibility and infectivity. *J. Cell Sci.*, **123**, 1191–1201.
10. Ayala, Y.M., Zago, P., D'Ambrogio, A., Xu, Y.F., Petrucelli, L., Buratti, E. and Baralle, F.E. (2008) Structural determinants of the cellular localization and shuttling of TDP-43. *J. Cell Sci.*, **121**, 3778–3785.
11. Colombrita, C., Zennaro, E., Fallini, C., Weber, M., Sommacal, A., Buratti, E., Silani, V. and Ratti, A. (2009) TDP-43 is recruited to stress granules in conditions of oxidative insult. *J. Neurochem.*, **111**, 1051–1061.
12. Freibaum, B.D., Chitta, R.K., High, A.A. and Taylor, J.P. (2010) Global analysis of TDP-43 interacting proteins reveals strong association with RNA splicing and translation machinery. *J. Proteome Res.*, **9**, 1104–1120.
13. Liu-Yesucevitz, L., Bilgutay, A., Zhang, Y.J., Vanderweyde, T., Citro, A., Mehta, T., Zaarur, N., McKee, A., Bowser, R., Sherman, M. *et al*. (2010) Tar DNA binding protein-43 (TDP-43) associates with stress granules: analysis of cultured cells and pathological brain tissue. *PLoS ONE*, **5**, e13250.
14. Dewey, C.M., Cenik, B., Sephton, C.F., Johnson, B.A., Herz, J. and Yu, G. (2012) TDP-43 aggregation in neurodegeneration: are stress granules the key? *Brain Res.*, **1462**, 16–25.
15. Li, Y.R., King, O.D., Shorter, J. and Gitler, A.D. (2013) Stress granules as crucibles of ALS pathogenesis. *J. Cell Biol.*, **201**, 361–372.
16. Wolozin, B. (2012) Regulated protein aggregation: stress granules and neurodegeneration. *Mol. Neurodegener.*, **7**, 56.
17. Nonaka, T., Arai, T., Buratti, E., Baralle, F.E., Akiyama, H. and Hasegawa, M. (2009) Phosphorylated and ubiquitinated TDP-43 pathological inclusions in ALS and FTLD-U are recapitulated in SH-SY5Y cells. *FEBS Lett.*, **583**, 394–400.
18. Guo, W., Chen, Y., Zhou, X., Kar, A., Ray, P., Chen, X., Rao, E.J., Yang, M., Ye, H., Zhu, L. *et al*. (2011) An ALS-associated mutation affecting TDP-43 enhances protein aggregation, fibril formation and neurotoxicity. *Nat. Struct. Mol. Biol.*, **18**, 822–830.
19. Choksi, D.K., Roy, B., Chatterjee, S., Yusuff, T., Bakhoum, M.F., Sengupta, U., Ambegaokar, S., Kayed, R. and Jackson, G.R. (2013) TDP-43 Phosphorylation by casein kinase Iε promotes oligomerization and enhances toxicity in vivo. *Hum. Mol. Genet.*, **23**, 1025–1035.
20. Li, H.Y., Yeh, P.A., Chiu, H.C., Tang, C.Y. and Tu, B.P. (2011) Hyperphosphorylation as a defense mechanism to reduce TDP-43 aggregation. *PLoS ONE*, **6**, e23075.
21. Zhang, Y.J., Gendron, T.F., Xu, Y.F., Ko, L.W., Yen, S.H. and Petrucelli, L. (2010) Phosphorylation regulates proteasomal-mediated degradation and solubility of TAR DNA binding protein-43 C-terminal fragments. *Mol. Neurodegener.*, **5**, 33.
22. Scotter, E.L., Vance, C., Nishimura, A.L., Lee, Y.B., Chen, H.J., Urwin, H., Sardone, V., Mitchell, J.C., Rogelj, B., Rubinsztein, D.C. *et al*. (2014) Differential roles of the ubiquitin proteasome system and autophagy in the clearance of soluble and aggregated TDP-43 species. *J Cell Sci*, **127**, 1263–1278.
23. Ling, S.C., Polymenidou, M. and Cleveland, D.W. (2013) Converging mechanisms in ALS and FTD: disrupted RNA and protein homeostasis. *Neuron*, **79**, 416–438.
24. Gendron, T.F., Rademakers, R. and Petrucelli, L. (2013) TARDBP mutation analysis in TDP-43 proteinopathies and deciphering the toxicity of mutant TDP-43. *J. Alzheimers Dis.*, **33**(Suppl. 1), S35–S45.

25. Dammer, E.B., Fallini, C., Gozal, Y.M., Duong, D.M., Rossoll, W., Xu, P., Lah, J.J., Levey, A.I., Peng, J., Bassell, G.J. *et al.* (2012) Coaggregation of RNA-binding proteins in a model of TDP-43 proteinopathy with selective RGG motif methylation and a role for RRM1 ubiquitination. *PLoS ONE*, **7**, e38658.
26. Barmada, S.J., Skibinski, G., Korb, E., Rao, E.J., Wu, J.Y. and Finkbeiner, S. (2010) Cytoplasmic mislocalization of TDP-43 is toxic to neurons and enhanced by a mutation associated with familial amyotrophic lateral sclerosis. *J. Neurosci.*, **30**, 639–649.
27. Igaz, L.M., Kwong, L.K., Xu, Y., Truax, A.C., Uryu, K., Neumann, M., Clark, C.M., Elman, L.B., Miller, B.L., Grossman, M. *et al.* (2008) Enrichment of C-terminal fragments in TAR DNA-binding protein-43 cytoplasmic inclusions in brain but not in spinal cord of frontotemporal lobar degeneration and amyotrophic lateral sclerosis. *Am. J. Pathol.*, **173**, 182–194.
28. Igaz, L.M., Kwong, L.K., Chen-Plotkin, A., Winton, M.J., Unger, T.L., Xu, Y., Neumann, M., Trojanowski, J.Q. and Lee, V.M. (2009) Expression of TDP-43 C-terminal fragments in vitro recapitulates pathological features of TDP-43 proteinopathies. *J. Biol. Chem.*, **284**, 8516–8524.
29. Xu, Z.S. (2012) Does a loss of TDP-43 function cause neurodegeneration? *Mol. Neurodegener.*, **7**, 27.
30. Yang, C., Wang, H., Qiao, T., Yang, B., Aliaga, L., Qiu, L., Tan, W., Salameh, J., McKenna-Yasek, D.M., Smith, T. *et al.* (2014) Partial loss of TDP-43 function causes phenotypes of amyotrophic lateral sclerosis. *Proc. Natl Acad. Sci. USA*, **111**, E1121–E1129.
31. Lee, E.B., Lee, V.M. and Trojanowski, J.Q. (2012) Gains or losses: molecular mechanisms of TDP43-mediated neurodegeneration. *Nat. Rev. Neurosci.*, **13**, 38–50.
32. Diaper, D.C., Adachi, Y., Sutcliffe, B., Humphrey, D.M., Elliott, C.J., Stepto, A., Ludlow, Z.N., Vanden Broeck, L., Callaerts, P., Dermaut, B. *et al.* (2013) Loss and gain of Drosophila TDP-43 impair synaptic efficacy and motor control leading to age-related neurodegeneration by loss-of-function phenotypes. *Hum. Mol. Genet.*, **22**, 1539–1557.
33. Halliday, G., Bigio, E.H., Cairns, N.J., Neumann, M., Mackenzie, I.R. and Mann, D.M. (2012) Mechanisms of disease in frontotemporal lobar degeneration: gain of function versus loss of function effects. *Acta Neuropathol.*, **124**, 373–382.
34. Kabashi, E., Lin, L., Tradewell, M.L., Dion, P.A., Bercier, V., Bourgouin, P., Rochefort, D., Bel Hadj, S., Durham, H.D., Vande Velde, C. *et al.* (2010) Gain and loss of function of ALS-related mutations of TARDBP (TDP-43) cause motor deficits in vivo. *Hum. Mol. Genet.*, **19**, 671–683.
35. Banerjee, A., Apponi, L.H., Pavlath, G.K. and Corbett, A.H. (2013) PABPN1: molecular function and muscle disease. *FEBS J.*, **280**, 4230–4250.
36. Kusters, B., van Hoeve, B.J., Schelhaas, H.J., Ter Laak, H., van Engelen, B.G. and Lammens, M. (2009) TDP-43 accumulation is common in myopathies with rimmed vacuoles. *Acta Neuropathol.*, **117**, 209–211.
37. Fan, X., Messaed, C., Dion, P., Laganiere, J., Brais, B., Karpati, G. and Rouleau, G.A. (2003) HnRNP A1 and A/B interaction with PABPN1 in oculopharyngeal muscular dystrophy. *Can. J. Neurol. Sci.*, **30**, 244–251.
38. Fronz, K., Guttinger, S., Burkert, K., Kuhn, U., Stohr, N., Schierhorn, A. and Wahle, E. (2011) Arginine methylation of the nuclear poly(a) binding protein weakens the interaction with its nuclear import receptor, transportin. *J. Biol. Chem.*, **286**, 32986–32994.
39. Kerwitz, Y., Kuhn, U., Lilie, H., Knoth, A., Scheuermann, T., Friedrich, H., Schwarz, E. and Wahle, E. (2003) Stimulation of poly(A) polymerase through a direct interaction with the nuclear poly(A) binding protein allosterically regulated by RNA. *EMBO J.*, **22**, 3705–3714.
40. Kuo, P.H., Doudeva, L.G., Wang, Y.T., Shen, C.K. and Yuan, H.S. (2009) Structural insights into TDP-43 in nucleic-acid binding and domain interactions. *Nucleic Acids Res.*, **37**, 1799–1808.
41. Song, J., McGivern, J.V., Nichols, K.W., Markley, J.L. and Sheets, M.D. (2008) Structural basis for RNA recognition by a type II poly(A)-binding protein. *Proc. Natl Acad. Sci. USA*, **105**, 15317–15322.
42. Abu-Baker, A., Laganiere, S., Fan, X., Laganiere, J., Brais, B. and Rouleau, G.A. (2005) Cytoplasmic targeting of mutant poly(A)-binding protein nuclear 1 suppresses protein aggregation and toxicity in oculopharyngeal muscular dystrophy. *Traffic*, **6**, 766–779.
43. Johnson, B.S., McCaffery, J.M., Lindquist, S. and Gitler, A.D. (2008) A yeast TDP-43 proteinopathy model: Exploring the molecular determinants of TDP-43 aggregation and cellular toxicity. *Proc. Natl Acad. Sci. USA*, **105**, 6439–6444.
44. Johnson, B.S., Snead, D., Lee, J.J., McCaffery, J.M., Shorter, J. and Gitler, A.D. (2009) TDP-43 is intrinsically aggregation-prone, and amyotrophic lateral sclerosis-linked mutations accelerate aggregation and increase toxicity. *J. Biol. Chem.*, **284**, 20329–20339.
45. Armakola, M., Hart, M.P. and Gitler, A.D. (2010) TDP-43 toxicity in yeast. *Methods*, **53**, 238–245.
46. Fallini, C., Bassell, G.J. and Rossoll, W. (2012) The ALS disease protein TDP-43 is actively transported in motor neuron axons and regulates axon outgrowth. *Hum. Mol. Genet.*, **21**, 3703–3718.
47. Zhang, Y.J., Xu, Y.F., Cook, C., Gendron, T.F., Roettges, P., Link, C.D., Lin, W.L., Tong, J., Castanedes-Casey, M., Ash, P. *et al.* (2009) Aberrant cleavage of TDP-43 enhances aggregation and cellular toxicity. *Proc. Natl. Acad. Sci. USA*, **106**, 7607–7612.
48. Liu-Yesucevitz, L., Lin, A.Y., Ebata, A., Boon, J.Y., Reid, W., Xu, Y. F., Kobrin, K., Murphy, G.J., Petrucelli, L. and Wolozin, B. (2014) ALS-linked mutations enlarge TDP-43-enriched neuronal RNA granules in the dendritic arbor. *J. Neurosci.*, **34**, 4167–4174.
49. Hanson, K.A., Kim, S.H., Wassarman, D.A. and Tibbetts, R.S. (2010) Ubiquilin modifies TDP-43 toxicity in a Drosophila model of amyotrophic lateral sclerosis (ALS). *J. Biol. Chem.*, **285**, 11068–11072.
50. Ihara, R., Matsukawa, K., Nagata, Y., Kunugi, H., Tsuji, S., Chihara, T., Kuranaga, E., Miura, M., Wakabayashi, T., Hashimoto, T. *et al.* (2013) RNA binding mediates neurotoxicity in the transgenic Drosophila model of TDP-43 proteinopathy. *Hum. Mol. Genet.*, **22**, 4474–4484.
51. Li, Y., Ray, P., Rao, E.J., Shi, C., Guo, W., Chen, X., Woodruff, E. A. 3rd, Fushimi, K. and Wu, J.Y. (2010) A Drosophila model for TDP-43 proteinopathy. *Proc. Natl Acad. Sci. USA*, **107**, 3169–3174.
52. Ritson, G.P., Custer, S.K., Freibaum, B.D., Guinto, J.B., Geffel, D., Moore, J., Tang, W., Winton, M.J., Neumann, M., Trojanowski, J.Q. *et al.* (2010) TDP-43 mediates degeneration in a novel Drosophila model of disease caused by mutations in VCP/p97. *J. Neurosci.*, **30**, 7729–7739.
53. Voigt, A., Herholz, D., Fiesel, F.C., Kaur, K., Muller, D., Karsten, P., Weber, S.S., Kahle, P.J., Marquardt, T. and Schulz, J.B. (2010) TDP-43-mediated neuron loss in vivo requires RNA-binding activity. *PLoS ONE*, **5**, e12247.
54. Estes, P.S., Boehringer, A., Zwick, R., Tang, J.E., Grigsby, B. and Zarnescu, D.C. (2011) Wild-type and A315T mutant TDP-43 exert differential neurotoxicity in a Drosophila model of ALS. *Hum. Mol. Genet.*, **20**, 2308–2321.

55. Brand, A.H. and Perrimon, N. (1993) Targeted gene expression as a means of altering cell fates and generating dominant phenotypes. *Development*, **118**, 401–415.
56. Benoit, B., Mitou, G., Chartier, A., Temme, C., Zaessinger, S., Wahle, E., Busseau, I. and Simonelig, M. (2005) An essential cytoplasmic function for the nuclear poly(A) binding protein, PABP2, in poly(A) tail length control and early development in Drosophila. *Dev Cell.*, **9**, 511–522.
57. Estes, P.S., Daniel, S.G., McCallum, A.P., Boehringer, A.V., Sukhina, A.S., Zwick, R.A. and Zarnescu, D.C. (2013) Motor neurons and glia exhibit specific individualized responses to TDP-43 expression in a Drosophila model of amyotrophic lateral sclerosis. *Dis. Model Mech.*, **6**, 721–733.
58. Kim, H.J., Raphael, A.R., LaDow, E.S., McGurk, L., Weber, R.A., Trojanowski, J.Q., Lee, V.M., Finkbeiner, S., Gitler, A.D. and Bonini, N.M. (2014) Therapeutic modulation of eIF2alpha phosphorylation rescues TDP-43 toxicity in amyotrophic lateral sclerosis disease models. *Nat. Genet.*, **46**, 152–160.
59. Li, S.H. and Li, X.J. (1998) Aggregation of N-terminal Huntingtin is dependent on the length of its glutamine repeats. *Hum. Mol. Genet.*, **7**, 777–782.
60. Bentmann, E., Neumann, M., Tahirovic, S., Rodde, R., Dormann, D. and Haass, C. (2012) Requirements for stress granule recruitment of fused in sarcoma (FUS) and TAR DNA-binding protein of 43kDa (TDP-43). *J. Biol. Chem.*, **287**, 23079–23094.
61. Bentmann, E., Haass, C. and Dormann, D. (2013) Stress granules in neurodegeneration–lessons learnt from TAR DNA binding protein of 43kDa and fused in sarcoma. *FEBS J.*, **280**, 4348–4370.
62. Geser, F., Martinez-Lage, M., Kwong, L.K., Lee, V.M. and Trojanowski, J.Q. (2009) Amyotrophic lateral sclerosis, frontotemporal dementia and beyond: the TDP-43 diseases. *J. Neurol.*, **256**, 1205–1214.
63. Polymenidou, M., Lagier-Tourenne, C., Hutt, K.R., Huelga, S. C., Moran, J., Liang, T.Y., Ling, S.C., Sun, E., Wancewicz, E., Mazur, C. *et al.* (2011) Long pre-mRNA depletion and RNA missplicing contribute to neuronal vulnerability from loss of TDP-43. *Nat. Neurosci.*, **14**, 459–468.
64. Baralle, M., Buratti, E. and Baralle, F.E. (2013) The role of TDP-43 in the pathogenesis of ALS and FTLD. *Biochem. Soc. Trans.*, **41**, 1536–1540.
65. Igaz, L.M., Kwong, L.K., Lee, E.B., Chen-Plotkin, A., Swanson, E., Unger, T., Malunda, J., Xu, Y., Winton, M.J., Trojanowski, J.Q. *et al.* (2011) Dysregulation of the ALS-associated gene TDP-43 leads to neuronal death and degeneration in mice. *J. Clin. Invest.*, **121**, 726–738.
66. Barmada, S.J., Serio, A., Arjun, A., Bilican, B., Daub, A., Ando, D.M., Tsvetkov, A., Pleiss, M., Li, X., Peisach, D. *et al.* (2014) Autophagy induction enhances TDP43 turnover and survival in neuronal ALS models. *Nat. Chem. Biol.*, **10**, 677–685.
67. Hino, H., Araki, K., Uyama, E., Takeya, M., Araki, M., Yoshinobu, K., Miike, K., Kawazoe, Y., Maeda, Y., Uchino, M. *et al.* (2004) Myopathy phenotype in transgenic mice expressing mutated PABPN1 as a model of oculopharyngeal muscular dystrophy. *Hum. Mol. Genet.*, **13**, 181–190.
68. Braun, R.J., Buttner, S., Ring, J., Kroemer, G. and Madeo, F. (2009) Nervous yeast: modeling neurotoxic cell death. *Trends Biochem. Sci.*, **35**, 135–144.
69. Armakola, M., Higgins, M.J., Figley, M.D., Barmada, S.J., Scarborough, E.A., Diaz, Z., Fang, X., Shorter, J., Krogan, N.J., Finkbeiner, S. *et al.* (2012) Inhibition of RNA lariat debranching enzyme suppresses TDP-43 toxicity in ALS disease models. *Nat. Genet.*, **44**, 1302–1309.
70. Ju, S., Tardiff, D.F., Han, H., Divya, K., Zhong, Q., Maquat, L.E., Bosco, D.A., Hayward, L.J., Brown, R.H. Jr., Lindquist, S. *et al.* (2011) A yeast model of FUS/TLS-dependent cytotoxicity. *PLoS Biol.*, **9**, e1001052.
71. Elden, A.C., Kim, H.J., Hart, M.P., Chen-Plotkin, A.S., Johnson, B.S., Fang, X., Armakola, M., Geser, F., Greene, R., Lu, M.M. *et al.* (2010) Ataxin-2 intermediate-length polyglutamine expansions are associated with increased risk for ALS. *Nature*, **466**, 1069–1075.
72. Jackson, K.L., Dayton, R.D., Orchard, E.A., Ju, S., Ringe, D., Petsko, G.A., Maquat, L.E. and Klein, R.L. (2014) Preservation of forelimb function by UPF1 gene therapy in a rat model of TDP-43-induced motor paralysis. *Gene Ther.*, **22**, 20–28.
73. Jackrel, M.E., DeSantis, M.E., Martinez, B.A., Castellano, L.M., Stewart, R.M., Caldwell, K.A., Caldwell, G.A. and Shorter, J. (2014) Potentiated Hsp104 variants antagonize diverse proteotoxic misfolding events. *Cell*, **156**, 170–182.
74. Casci, I. and Pandey, U.B. (2014) A fruitful endeavor: modeling ALS in the fruit fly. *Brain Res.*, **1607**, 47–74.
75. Twyffels, L., Gueydan, C. and Kruys, V. (2014) Transportin-1 and transportin-2: protein nuclear import and beyond. *FEBS Lett.*, **588**, 1857–1868.
76. Mallet, P.L. and Bachand, F. (2013) A proline-tyrosine nuclear localization signal (PY-NLS) is required for the nuclear import of fission yeast PAB2, but not of human PABPN1. *Traffic*, **14**, 282–294.
77. Arrasate, M., Mitra, S., Schweitzer, E.S., Segal, M.R. and Finkbeiner, S. (2004) Inclusion body formation reduces levels of mutant huntingtin and the risk of neuronal death. *Nature*, **431**, 805–810.
78. Vanden Broeck, L., Callaerts, P. and Dermaut, B. (2014) TDP-43-mediated neurodegeneration: towards a loss-of-function hypothesis? *Trends Mol. Med.*, **20**, 66–71.
79. Wu, L.S., Cheng, W.C. and Shen, C.K. (2012) Targeted depletion of TDP-43 expression in the spinal cord motor neurons leads to the development of amyotrophic lateral sclerosis-like phenotypes in mice. *J. Biol. Chem.*, **287**, 27335–27344.
80. Iguchi, Y., Katsuno, M., Niwa, J., Takagi, S., Ishigaki, S., Ikenaka, K., Kawai, K., Watanabe, H., Yamanaka, K., Takahashi, R. *et al.* (2013) Loss of TDP-43 causes age-dependent progressive motor neuron degeneration. *Brain*, **136**, 1371–1382.
81. Fischer, L.R., Culver, D.G., Tennant, P., Davis, A.A., Wang, M., Castellano-Sanchez, A., Khan, J., Polak, M.A. and Glass, J.D. (2004) Amyotrophic lateral sclerosis is a distal axonopathy: evidence in mice and man. *Exp. Neurol.*, **185**, 232–240.
82. Yang, C., Tan, W., Whittle, C., Qiu, L., Cao, L., Akbarian, S. and Xu, Z. (2010) The C-terminal TDP-43 fragments have a high aggregation propensity and harm neurons by a dominant-negative mechanism. *PLoS ONE*, **5**, e15878.
83. Budini, M., Romano, V., Quadri, Z., Buratti, E. and Baralle, F. E. (2014) TDP-43 loss of cellular function through aggregation requires additional structural determinants beyond its C-terminal Q/N prion-like domain. *Hum. Mol. Genet.*, **24**, 9–20.
84. Buratti, E., Dörk, T., Zuccato, E., Pagani, F., Romano, M. and Baralle, F.E. (2001) Nuclear factor TDP-43 and SR proteins promote in vitro and in vivo CFTR exon 9 skipping. *EMBO J.*, **20**, 1774–1784.
85. Fan, X., Dion, P., Laganiere, J., Brais, B. and Rouleau, G.A. (2001) Oligomerization of polyalanine expanded PABPN1 facilitates nuclear protein aggregation that is associated with cell death. *Hum. Mol. Genet.*, **10**, 2341–2351.
86. Apponi, L.H., Corbett, A.H. and Pavlath, G.K. (2013) Control of mRNA stability contributes to low levels of nuclear poly(A)

binding protein 1 (PABPN1) in skeletal muscle. *Skelet. Muscle*, **3**, 23.
87. Apponi, L.H., Leung, S.W., Williams, K.R., Valentini, S.R., Corbett, A.H. and Pavlath, G.K. (2010) Loss of nuclear poly(A)-binding protein 1 causes defects in myogenesis and mRNA biogenesis. *Hum. Mol. Genet.*, **19**, 1058–1065.
88. McDonald, K.K., Aulas, A., Destroismaisons, L., Pickles, S., Beleac, E., Camu, W., Rouleau, G.A. and Vande Velde, C. (2011) TAR DNA-binding protein 43 (TDP-43) regulates stress granule dynamics via differential regulation of G3BP and TIA-1. *Hum. Mol. Genet.*, **20**, 1400–1410.
89. Nedelsky, N.B., Todd, P.K. and Taylor, J.P. (2008) Autophagy and the ubiquitin-proteasome system: collaborators in neuroprotection. *Biochim. Biophys. Acta.*, **1782**, 691–699.
90. Wang, I.F., Guo, B.S., Liu, Y.C., Wu, C.C., Yang, C.H., Tsai, K.J. and Shen, C.K. (2012) Autophagy activators rescue and alleviate pathogenesis of a mouse model with proteinopathies of the TAR DNA-binding protein 43. *Proc. Natl Acad. Sci. USA*, **109**, 15024–15029.
91. Lee, B.H., Lee, M.J., Park, S., Oh, D.C., Elsasser, S., Chen, P.C., Gartner, C., Dimova, N., Hanna, J., Gygi, S.P. *et al.* (2010) Enhancement of proteasome activity by a small-molecule inhibitor of USP14. *Nature*, **467**, 179–184.
92. Wang, X., Fan, H., Ying, Z., Li, B., Wang, H. and Wang, G. (2010) Degradation of TDP-43 and its pathogenic form by autophagy and the ubiquitin-proteasome system. *Neurosci. Lett.*, **469**, 112–116.
93. Alberti, S., Gitler, A.D. and Lindquist, S. (2007) A suite of Gateway cloning vectors for high-throughput genetic analysis in Saccharomyces cerevisiae. *Yeast*, **24**, 913–919.
94. Fallini, C., Bassell, G.J. and Rossoll, W. (2010) High-efficiency transfection of cultured primary motor neurons to study protein localization, trafficking, and function. *Mol. Neurodegener.*, **5**, 17.
95. Fallini, C., Zhang, H., Su, Y., Silani, V., Singer, R.H., Rossoll, W. and Bassell, G.J. (2011) The survival of motor neuron (SMN) protein interacts with the mRNA-binding protein HuD and regulates localization of poly(A) mRNA in primary motor neuron axons. *J. Neurosci.*, **31**, 3914–3925.
96. Messaed, C., Dion, P.A., Abu-Baker, A., Rochefort, D., Laganiere, J., Brais, B. and Rouleau, G.A. (2007) Soluble expanded PABPN1 promotes cell death in oculopharyngeal muscular dystrophy. *Neurobiology of Disease*, **26**, 546–557.
97. Schneider, C.A., Rasband, W.S. and Eliceiri, K.W. (2012) NIH Image to ImageJ: 25 years of image analysis. *Nat. Methods*, **9**, 671–675.